Multi-omics profiling establishes the polypharmacology of FDA Approved CDK4/6 inhibitors and the potential for differential clinical activity

Marc Hafner[*,1,3], **Caitlin Elizabeth Mills**[*,1], **Kartik Subramanian**[1], **Chen Chen**[1], **Mirra Chung**[1], **Sarah Ann Boswell**[1], **Robert A. Everley**[1], **Changchang Liu**[1], **Charlotte Sanden Walmsley**[2], **Dejan Juric**[1,2,φ], **Peter Karl Sorger**[1,†,φ]

[1]Laboratory of Systems Pharmacology, Department of Systems Biology, Harvard Medical School, Boston, MA 02115

[2]Termeer Center for Targeted Therapies, Massachusetts General Hospital Cancer Center, Boston, MA 02114

SUMMARY

The target profiles of many drugs are established early in their development and are not systematically revisited at the time of FDA approval. Thus, it is often unclear whether therapeutics with the same nominal targets but different chemical structures are functionally equivalent. In this paper we use five different phenotypic and biochemical assays to compare approved inhibitors of cyclin-dependent kinases 4/6 – collectively regarded as breakthroughs in the treatment of hormone receptor-positive breast cancer. We find that transcriptional, proteomic, and phenotypic changes induced by palbociclib, ribociclib, and abemaciclib differ significantly; abemaciclib in particular has advantageous activities partially overlapping those of alvocidib, an older polyselective CDK inhibitor. In cells and mice, abemaciclib inhibits kinases other than CDK4/6 including CDK2/Cyclin A/E – implicated in resistance to CDK4/6 inhibition – and CDK1/Cyclin B. The multi-faceted experimental and computational approaches described here therefore uncover under-appreciated differences in CDK4/6 inhibitor activities with potential importance in treating human patients.

Keywords

Cancer therapeutics; kinase inhibitors; palbociclib; ribociclib; abemaciclib; breast cancer; CDK4/6 inhibitors; drug profiling; drug mechanisms of action

INTRODUCTION

Progression through the cell cycle is controlled by more than a dozen distinct protein complexes involving cyclins and cyclin-dependent kinases (CDKs). Because dysregulation of the cell cycle is a hallmark of cancer, several generations of CDK inhibitors have been tested as potential therapeutic agents. However, identifying CDK inhibitors that are more active on tumor than normal cells has been a challenge and it is only recently that CDK4/6 inhibitors have emerged as promising therapies, particularly in breast cancer. CDK4 and CDK6 bind cyclin D early in the G1 phase of the cell cycle and phosphorylate the retinoblastoma protein (pRb). pRb is then hyper-phosphorylated by CDK2/cyclin E, relieving its inhibitory activities against transcription factors of the E2F family and allowing for S phase entry. Later in the cell cycle, CDK2/cyclin A and CDK1 in complex with cyclin A and B promote entry and progression through G2 and mitosis. Multiple genetic changes in cancer cells disrupt critical steps in cell cycle regulation: amplification of CDK4, CDK6, cyclin D, or cyclin E are common in solid tumors including breast cancers (Asghar et al., 2015; Balko et al., 2014). Also common are deficiencies in pRb function, which cause unregulated S phase entry, and deletion of the CDK4/6 inhibitor p16 (encoded by *CDKN2A*) (Asghar et al., 2015; Franco et al., 2014).

First generation pan-CDK inhibitors active against cell cycle regulators such as CDK1/2/4/6 and transcriptional regulators such as CDK9 arrest cells in both G1 and G2, and are broadly cytotoxic. Consequently, their clinical development has been challenged by poor therapeutic windows (Asghar et al., 2015). Subsequent generations of CDK inhibitors have been designed to inhibit specific CDK proteins (or subfamilies). In February 2015, the CDK4/6 inhibitor, palbociclib (PD0332991; Ibrance®) (Cristofanilli et al., 2016) received FDA approval for management of hormone receptor-positive (HR+) metastatic breast cancer (MBC) (Finn et al., 2009; O'Leary et al., 2016). Clinical trials of the CDK4/6 inhibitors, ribociclib (LEE011; KISQALI®) (Hortobagyi et al., 2016) and abemaciclib (LY2835219; Verzenio®) (Dickler et al., 2016; Sledge et al., 2017) also demonstrated substantial improvements in progression-free survival in HR+ metastatic breast cancer (Cristofanilli et al., 2016; Griggs and Wolff, 2017) leading to their approval by the FDA. CDK4/6 inhibitors are currently regarded as some of the most promising new drugs for the treatment of HR+ breast cancer and are also being tested against other malignancies (Goel et al., 2016; Lim et al., 2016; McCain, 2015; Patnaik et al., 2016a).

As observed with many other targeted therapies, acquired resistance to CDK4/6 inhibitors develops over time and nearly all initially responsive patients ultimately progress (Sherr et al., 2016). Resistance to CDK4/6 inhibitors is associated with multiple genomic alterations including amplification of Cyclin E, which promotes CDK2-dependent phosphorylation of pRb, amplification of CDK6, and loss of pRb function (Asghar et al., 2015; Yang et al.,

2017). High expression of cyclin E is also associated with high CDK2 activity post-mitosis, which appears to bypass a requirement for CDK4/6 for cell cycle reentry (Asghar et al., 2017).

Despite having the same nominal targets and similar clinical indications, emerging evidence suggests that palbociclib, ribociclib, and abemaciclib differ in the clinic: abemaciclib in particular has been reported to have unique single-agent activities and distinct adverse effects (O'Brien et al., 2018; Patnaik et al., 2016b). The three drugs are dosed differently, have different pharmacokinetics, and are reported to differ with respect to target selectivity (Chen et al., 2016; Cousins et al., 2017; Gelbert et al., 2014; Kim et al., 2018; Sumi et al., 2015). Among abemaciclib secondary targets examined to date, inhibition of DYRK/HIPK kinases is thought to contribute to cellular cytotoxicity (Knudsen et al., 2017); inhibition of GSK3α/β can activate WNT signaling (Cousins et al., 2017); inhibition of CDK9 is thought to be therapeutically unimportant (Torres-guzmán et al., 2017); however, overall the biological significance of differences in potency against primary CDK4/6 targets and secondary targets remains largely unexplored.

The target profiles of most clinical compounds are established relatively early in their development and are not necessarily revised at the time of approval. This is further complicated in the case of kinase inhibitors by the use of different measurement technologies to assess selectivity and the steady evolution of these technologies over the course of development of a single drug. By directly comparing the target profiles and biological activities of palbociclib, ribociclib and abemaciclib, as well as an earlier generation pan-CDK inhibitor, alvocidib (flavopiridol), we sought to address three related questions: (i) are the three approved CDK4/6 inhibitors interchangeable with respect to biochemical and cell-based activities; (ii) is there a possibility that tumors that have become resistant to one CDK4/6 inhibitor remain responsive to another inhibitor; and (iii) what are the relative merits of different approaches to characterizing the target spectra of kinase inhibitors?

In this paper we report the analysis of the clinically-approved CDK4/6 inhibitors using five experimental approaches that provide complementary insights into drug mechanisms of action: (i) mRNA sequencing of drug-perturbed cells, (ii) phosphoproteomics using mass spectrometry, (iii) GR-based dose-response measurement of cellular phenotypes (Hafner et al., 2016), (iv) mRNA sequencing of drug-treated xenograft tumors and (v) *in vitro* analysis for inhibitory activity using three different approaches: activity assays with recombinant enzymes; kinome-wide profiling using the commercial KINOMEscan platform from DiscoverX (Fabian et al., 2005); and kinase enrichment proteomics based on affinity purification on kinobeads (Duncan et al., 2012). We find that the five experimental approaches provide different but complementary views of target coverage and demonstrate that palbociclib, ribociclib, and abemaciclib have substantial differences in secondary targets and biological activities in breast cancer cell lines of varying genotypes. Multiple lines of evidence, including an *in vivo* xenograft model and preliminary data on patients and patient-derived cell lines treated with abemaciclib, suggest that the unique activities of abemaciclib arise from inhibition of kinases in addition to CDK4/6, notably CDK1 and CDK2, and may be therapeutically advantageous.

RESULTS

Approved CDK4/6 inhibitors induce distinct molecular signatures in breast cancer cells

To compare the mechanisms of action of palbociclib, ribociclib, and abemaciclib we performed transcriptional profiling (mRNA-seq) on a panel of seven breast cancer cell lines following 6 or 24 hours of exposure to 0.3, 1, or 3 μM of drug (Figure 1a and Table S1). In all but pRb-deficient BT-549 cells, treatment with any of the three drugs gave rise to a signature (signature 1; Figure 1a in red) comprising 87 significantly down-regulated genes (FDR < 0.2). In addition, treatment of cells with abemaciclib in the low micromolar range (gray box in Figures 1a) induced a second transcriptional signature (signature 2; Figure 1a in cyan) comprising 688 significantly down-regulated genes (FDR < 0.2) that was absent from ribociclib-exposed cells and only weakly present in cells exposed to palbociclib. We queried the Broad Connectivity Map (CMAP) (Lamb et al., 2006) with the two sets of down-regulated genes to determine which drug-induced changes they most closely matched. For signature 1, palbociclib and inhibitors of MEK (MAP kinase kinase) were the strongest hits (ribociclib and abemaciclib are absent from the CMAP dataset; Figure 1b and Table S1). Like CDK4/6 inhibition, MEK inhibition is anti-mitogenic in breast cancer cells, causing cells to arrest at the G1/S transition (Caunt et al., 2015; Meloche and Pouysségur, 2007). Gene set enrichment analysis showed that signature 1 was enriched for genes in the set *Reactome "Cell Cycle"* (p=9.0×10^{-50}); it therefore appears to reflect cell cycle arrest in G1 (O'Leary et al., 2016). When signature 2 was compared to CMAP, the strongest hits were alvocidib and other pan-CDK inhibitors (Figure 1c and Table S1), suggesting that this signature arises from inhibition of CDKs other than CDK4 and CDK6. We defined the "G1-arrest score" as the absolute mean $\log_2$ fold-change in the expression of all genes comprising signature 1 and the "pan-CDK score" as the absolute mean $\log_2$ fold-change in expression of genes in signature 2. The G1-arrest score was high for all three drugs (Figure S1) whereas the strength of the pan-CDK score varied with drug and dose; it was highest for abemaciclib above 0.3 μM and lowest for ribociclib. Palbociclib exposure was associated with intermediate scores (Figure 1d).

To better understand the origins of the pan-CDK signature, we collected mRNA-seq data from a larger set of conditions using the high-throughput, low-cost RNA sequencing method 3' Digital Gene Expression (DGE-seq) (Soumillon et al., 2014). Seven cell lines, including two that are pRB-deficient (BT-549 and PDX-1258), were exposed for 6 hours to palbociclib, ribociclib, or abemaciclib or to alvocidib (which inhibits CDK1/2/4/6/9); data were collected in triplicate at four CDK4/6 inhibitor concentrations and two alvocidib concentrations. Differential expression of genes in signatures 1 and 2 (as defined above) was then used to compute G1-arrest and pan-CDK scores for each condition (Figure 2, Table S1). From these data we found that the strength of the average pan-CDK score was ordered as follows: alvocidib > abemaciclib > palbociclib > ribociclib (Figure 2, x-axis). For abemaciclib and alvocidib the pan-CDK score was strongly dose dependent (r=0.78, p=9.3×10^{-7} and r=0.76, p=1.5×10^{-3} respectively) as were the G1 arrest scores for all four drugs. Notably, the pan-CDK score for 0.1 μM and 1 μM alvocidib across all cell lines (green) substantially overlapped abemaciclib at 1 μM and 3 μM (blue).

In pRb-deficient lines, only four genes in the G1 signature were differentially regulated by ribociclib (two-sided Fisher exact test p=2×10^{-4} as compared to pRb-proficient lines) consistent with the hypothesis that a pure CDK4/6 inhibitor should be inactive in cells lacking pRb, the primary substrate of CDK4/6 kinases. Overall, G1 arrest scores were lower in pRb-deficient than in pRb-proficient cell lines (0.25 vs. 0.73 on average) but they were not zero. This likely arises because pan-CDK and G1 arrest signatures are not orthogonal and inhibition of CDKs contributes to both. These RNA-seq data strongly suggest that palbociclib, ribociclib, and abemaciclib have different target spectra in breast cancer cells. Moreover, like alvocidib, abemaciclib is biologically active in pRb-deficient cells, as assessed by changes in gene transcription.

Effects of CDK4/6 inhibitors on the activity of CDK/cyclin complexes

To study the effects of CDK4/6 inhibitors on the phosphoproteome we performed isobaric (TMT) tag based liquid-chromatography mass spectrometry (LC/MS) (McAlister et al., 2012). MCF7 cells were treated with DMSO, palbociclib, or abemaciclib for one hour (to focus on immediate-early changes in the phosphoproteome) and a total of 9958 phosphopeptides were detected across all samples; among these phosphopeptides, 739 were down-regulated in the presence of palbociclib and 2287 in the presence of abemaciclib ($\log_2$ fold-change > 1.5; Figure 3a, Table S2). Enrichment analysis (Drake et al., 2012) involving known kinase-substrate relationships (see Methods) was used to infer changes in the activities of upstream kinases potentially accounting for observed changes in the phosphoproteome. The inferred activities for CDK4, CDK6, and Aurora A/B kinases (AURKA/B) were significantly lower in cells treated with either palbociclib or abemaciclib than a DMSO-only control whereas the inferred activities of CDK1, CDK2, and CaM-kinase II subunit alpha (CAMKIIα) were lower only in cells treated with abemaciclib (Figure 3b, Table S2).

Kinase inference suggests that palbociclib and abemaciclib down-regulate the activities of multiple kinases other than CDK4 and CDK6. However, this conclusion has several caveats, most importantly, that kinase inhibitors can act indirectly, for example, by blocking the activity of an upstream kinase in a multi-step cascade or by arresting cells at a point in the cell cycle at which some kinases are not normally active (CDKs for example). Second, even when using state-of-the-art mass spectrometers and methods, less than 10% of the total phosphoproteome can be analyzed in any single sample, making kinase-inference subject to statistical error. Third, there exists a poorly established many-to-many mapping between kinases and substrates, necessitating predictive models based on motif signatures and binding probabilities, all with associated uncertainties. Because of these limitations we consider kinase inference to be a semi-quantitative method: large differences across drugs are likely meaningful but dose-response relationships can be hard to capture.

To distinguish direct and indirect effects of kinase inhibitors on the phosphoproteome we performed three different types of *in vitro* assays. First, we used the commercial KINOMEscan assay, which measures binding between members of a 468 DNA-tagged recombinant kinase library and an immobilized ATP-like ligand; the assay is performed in the presence and absence of an ATP-competitive drug (Fabian et al., 2005). KINOMEscan

profiling showed that ribociclib is the most selective CDK4/6 inhibitor and abemaciclib the least (Figure 3c, Figure S2a–b and Table S3). KINOMEscan assays have previously been performed on CDK4/6 inhibitors (Chen et al., 2016; Gelbert et al., 2014); our data agree with earlier findings.

Several CDKs are not found in the KINOMEscan library (e.g. CDK1, CDK6) or are not complexed with cyclins (e.g. CDK2); therefore, we used a second method to obtain kinome profiles: multiplexed inhibitor bead mass spectrometry (MIB/MS) (Donnella et al., 2018; Duncan et al., 2012). In this approach, a cell lysate is mixed with beads conjugated to pan-kinase inhibitors in the presence and absence of a test drug and the levels of bound kinases are then determined by mass spectrometry (Figure 3d, Table S4); to generate a lysate with the greatest number of expressed kinases, we mixed several cell types (Médard et al., 2015). We detected 164 kinases, including 13 CDKs in the unfractionated extract by TMT LC/MS, and found that ribociclib, palbociclib, and abemaciclib all bound to CDK4 and CDK6. In addition, abemaciclib bound to CDK1, CDK2, CDK7, CDK9, GSK3α/β and CAMKIIγ/δ. These results agree well with data for abemaciclib recently published by Cousins et al. (Spearman's $\rho = 0.62$, $P = 8.9 \times 10^{-16}$) (Cousins et al., 2017). Moreover, when KINOMEscan data (obtained in the presence of 1 μM abemaciclib) and MIB data (obtained with 10 μM abemaciclib) were compared, 19 of 25 kinases strongly inhibited in the KINOMEscan (> 90% inhibition) and also present in cell extracts were significantly reduced in binding to MIBs (log2 fold change > 1.5), demonstrating good reproducibility between different types of assays. We conclude that ribociclib is the most selective CDK4/6 inhibitor tested and abemaciclib the least, with a dose-dependent increase in the number of targets significantly inhibited by abemaciclib from 4 at 0.1 μM drug to 13 at 1 μM and 28 at 10 μM.

As a third approach, we performed *in vitro* kinase activity assays at 10 concentrations (using SelectScreen technology by Thermo Fisher and HotSpot technology by Reaction Biology; see STAR Methods). Drugs were tested on the kinases and kinase-cyclin complexes that we identified as potential abemaciclib targets by transcriptional, phosphoproteomic, or kinase profiling assays. The data showed that abemaciclib was the most potent inhibitor of CDK4 and CDK6 of the three drugs tested and that it was also active against multiple kinases that were not inhibited, or were only weakly inhibited, by palbociclib or ribociclib (Figure 3e, Figure S3 and Table S5). These kinases include CDK2/cyclin A/E, CDK1/cyclin B, CDK7/cyclin H, CDK9/cyclin K/T1, CAMKIIα/β/γ, and GSK-3α/β (Figure 3e, Figure S3). Compared to the first-generation CDK inhibitor alvocidib, abemaciclib had similar potency against CDK2/cyclin A/E but was ~10-fold less potent against CDK1/cyclin B, CDK7/cyclin H, and CDK9/cyclin K/T1 (potentially explaining the improved toxicity profile of abemaciclib relative to pan-CDK inhibitors), whereas ribociclib and palbociclib were at least another order of magnitude less potent than abemaciclib against these secondary targets. The potency of the three drugs against CDK4 vs. CDK6 was dependent on the cyclin partner and the assay, but generally differed by no more than 3-fold (Table S5).

Results from KINOMEscan, MIB/MS, and SelectScreen assays performed *in vitro* were largely concordant with mRNA-seq and phosphoproteome profiling with a few notable exceptions (Figure 3f). CDK1 and CDK6 were absent from the KINOMEscan panel and CDK2 was not found to be a target, probably because the appropriate cyclin was absent and

cyclin binding changes CDK2 activity (Echalier et al., 2014). Such a false-negative result in the widely used KINOMEscan assay may explain why the activity of abemaciclib against CDK2-cyclin A/E is under-appreciated. Biochemical assays showed that abemaciclib was inactive against other kinases such as AURKA/B, and PAK1 (Figure S3a) and the down-regulation inferred from phosphoproteomic data most likely reflects an indirect effect: arrest of cells in G1 by CDK4/6 inhibition is expected to block normal phosphorylation of AURKA/B, and PAK1 in G2/M phase. Thus, it was only by combining multiple *in vitro* and cell-based assays that a complete picture of kinase inhibitor activities was obtained (Figure 3f).

Comparing CDK4/6 inhibitors in breast cancer cell lines

To compare the biological activities of CDK4/6 inhibitors, we acquired dose-response curves in 34 breast cancer cell lines spanning all clinical subtypes and computed GR values (Figure 4a and Table S6) which distinguish between drug-induced cell cycle arrest and cell death while correcting for artifactual differences in drug sensitivity arising from variability in proliferation rates (Hafner et al., 2016, 2017a). Both palbociclib and abemaciclib elicited cytostatic responses with GR_{50} values in the 10–100 nM range (Table S6). Potency was highly correlated between the drugs (Spearman's $\rho = 0.91$, $P = 5.7 \times 10^{-14}$) with abemaciclib ~5.5-fold more potent on average at inducing cytostasis (t-test $P = 5.3 \times 10^{-7}$); this difference is consistent with a 3-fold difference between palbociclib and abemaciclib in *in vitro* IC_{50} values for CDK4/6 kinase activity (Figure 3e). Efficacy at 0.1 μM drug, as measured by GR value, varied between 0 (complete cytostasis) and 0.76 (weak growth inhibition) in pRb-proficient cell lines but was similar for palbociclib and abemaciclib, showing that at these concentrations the drugs induce similar phenotypic effects and only fractionally inhibit cell proliferation. In pRb-deficient cell lines, palbociclib was inactive at all doses and abemaciclib had little or no effect below 0.3 μM (yellow lines Figure 4a). The cytostatic response observed at lower abemaciclib doses and all doses of palbociclib is most likely a result of CDK4/6 inhibition.

However, abemaciclib also elicited a second response at doses greater than 0.3 μM; this response was characterized by negative GR values and cell death (see Methods; Figure 4a). As a result, the complete dose-response behavior of abemaciclib was significantly better fitted in most cell lines by the product of two sigmoidal curves (Figure 4b, Figure S4, and Methods). The mid-point of the second response curve was offset to a similar degree as *in vitro* dose-response curves for CDK1/2 vs. CDK4/6 inhibition (Table S5). This behavior is consistent with inhibition of two sets of targets: CDK4/6 at low dose – resulting in G1 arrest; and kinases such as CDK1/2 above 0.3 μM – resulting in cell death. At all doses tested in all cell lines, responses to palbociclib and ribociclib were purely cytostatic (GR > 0). As a result, abemaciclib was substantially more efficacious than palbociclib in inhibiting and killing pRb-proficient cells of all subtypes, having a GR_{max} value on average 0.52 below that of palbociclib (t-test $P=4.5 \times 10^{-9}$; Table S6).

A search of 30 cell cycle regulators for genes whose mRNA expression levels could discriminate between responsiveness to 3 μM palbociclib and abemaciclib in the 26 pRb-proficient cell lines yielded a high-performing multi-linear model involving only four genes

($q^2 = 0.85$, $P = 2.9\times10^{-6}$ by leave-one-out cross validation; Figures 4c–d and S4). The genes were CCNE1 (cyclin E1), which has been implicated in palbociclib resistance (Sherr et al., 2016; Turner et al., 2019), CDKN1A (p21 – an inhibitor of CDK2/4/6), CDK9 (a target of abemaciclib and pan-CDK inhibitors), and CDKL5 (cyclin-dependent kinase-like 5). Our data showed CDKL5 to be strongly inhibited by abemaciclib (IC_{50} ~ 18 nM in vitro) but not by palbociclib or ribociclib (IC_{50}>3 μM or >10 μM respectively; Table S5). Thus, differences in the efficacy of CDK4/6 inhibitors on cell lines are related to the expression levels of genes targeted uniquely by abemaciclib.

Abemaciclib blocks cells in the G2 phase of the cell cycle

Consistent with the known biology of CDK4/6 inhibition, abemaciclib, ribociclib, and palbociclib all suppressed pRb phosphorylation and arrested cells in G1 (Figure 5). The 3-fold difference in drug concentration needed to induce arrest matched measured differences in potency in biochemical assays (with abemaciclib the most potent and ribociclib the least; Figure 3e). A fraction of cells treated with abemaciclib also arrested in G2 rather than G1, particularly at drug concentrations of 0.3 μM and above (Figure 5, Figure S5), a possible consequence of inhibition of CDK1 and CDK2, whose activities are required for progression through S-phase and mitosis. Treating pRb-deficient cells with ribociclib or palbociclib had no effect on cell cycle distribution whereas treatment with abemaciclib caused cells to accumulate in G2, consistent with an abemaciclib-induced cell cycle arrest independent of CDK4/6 (Figure 5, Figure S5).

Assaying abemaciclib polypharmacology in xenograft tumors

When a drug inhibits multiple targets with different potencies the question arises whether both primary and secondary targets can be engaged at doses achievable *in vivo*. When we compared G1-arrest and pan-CDK signature scores and cellular phenotypes across a range of abemaciclib doses in multiple cell lines, we found that pan-CDK scores were significant only above 0.3 μM (P=2.1×10^{-4}, ranksum test) and cytotoxicity was observed in pRb-deficient cells only at concentrations of 1 μM and above. This compares well with a maximum serum concentration in humans (C_{max}) for abemaciclib of 0.5 μM to 1 μM when active metabolites are included (Burke et al., 2016; Patnaik et al., 2016a). As a direct test of *in vivo* activity we generated MCF-7 xenografts in nude mice and exposed them to CDK4/6 inhibitors at a range of doses. When tumors reached ~300 mm^3, animals were randomly assigned to treatment groups and treated daily for 4 days with a vehicle-only control or 150 mg/kg ribociclib, 150 mg/kg palbociclib or 25–150 mg/kg abemaciclib, doses previously shown to be effective in xenografts (Fry et al., 2004; Gelbert et al., 2014; O'Brien et al., 2014). Animals were euthanized and tumors divided into two samples; one was fixed in formaldehyde and paraffin embedded and the other processed for mRNA-sequencing. FFPE specimens were imaged by immunofluorescence using vimentin and E-cadherin staining to distinguish tumor cells from mouse stroma.

We found that all conditions tested resulted in a significant reduction in the fraction of p-pRb positive cells (Dunnett's multiple comparison $P < 0.0001$) providing pharmacodynamic evidence that all tumors were exposed to drug at active concentrations (Figure 6a). mRNA-seq data showed that all three drugs induced a G1-arrest signature (Figure 6b, Table S1), the

strength of which was correlated with the degree of p-pRb inhibition (Spearman's $\rho =$ -0.80, $P = 1.1 \times 10^{-10}$). Furthermore, at doses above 100 mg/kg, abemaciclib (but not ribociclib or palbociclib) also induced a strong pan-CDK signature (Figure 6b). These data provide *in vivo* confirmation that abemaciclib can engage targets other than CDK4 and CDK6, recapitulating data on the drug's off-target activity in cell culture.

Cross-resistance between abemaciclib and palbociclib or ribociclib is incomplete

As previously described (Asghar et al., 2017; Herrera-Abreu et al., 2016), cells adapt to CDK4/6 inhibition over time. Within 48 hours of exposure to palbociclib or ribociclib we found that cells re-entered the cell cycle and acquired a p-pRb positive state at drug concentrations as high as 3.16 μM (Figure 5). In contrast, pRb phosphorylation remained low in cells exposed to 1 μM or more abemaciclib (Figure 5a) with ongoing cell death and no evidence of adaptation five days after drug exposure (Figure 7a, Figure S6 and Table S6). In studies designed to assess long-term adaptation to drug, we observed that breast cancer cells grown for several months in the presence of 1 μM palbociclib had higher cyclin E (CCNE1) and lower pRb levels than parental cells (Figure 7b). These palbociclib-adapted cells were cross-resistant to ribociclib (Figure 7c, Figure S7a–b and Table S6) but sensitive to abemaciclib at doses of 1 μM and above, consistent with the ability of abemaciclib to target kinases not inhibited by palbociclib.

We observed similar differences in a cell line established from a patient with advanced/metastatic HR+/Her2- breast cancer whose disease had progressed following eight months on ribociclib/letrozole. The tumor lacked pRb by immunohistochemistry (Figure S7c) as did the derived cell line (MGH312; Figure S7d). The tumor cells were responsive to abemaciclib as judged by inhibition of cell proliferation and induction of cell death but were completely resistant to palbociclib or ribociclib even at high doses (Figure 7d and Table S6). The potential for abemaciclib to benefit this patient remains unknown because she is now deceased and was never treated with abemaciclib.

We also report the case of a 75 year-old woman with ER+(>10%)/PR+(1%−10%)/HER2- metastatic breast cancer with liver involvement (Figure 7e). The patient received fulvestrant (500mg IM on days 1, 15, 29 and once monthly thereafter) and palbociclib (125mg PO daily) for 20 months. Her liver lesion initially decreased in size based on complete radiographic disappearance of the target lesion after seven months of therapy. The same liver lesion reappeared at the time of disease progression while the patient was still on fulvestrant plus palbociclib. She was subsequently switched to single-agent abemaciclib (200 mg PO BID) as the immediate next line of therapy, resulting in a decrease of the same lesion after three months of abemaciclib. At the time of submission, the patient has been on abemaciclib for 12 months and is continuing to be treated. Based on these data, we propose that abemaciclib may have clinically useful activities in a subset of tumors that are not responsive, or have become resistant, to more selective CDK4/6 inhibitors. Our results also provide a rationale for clinical studies in which abemaciclib is initiated following progression on palbociclib or ribociclib.

DISCUSSION

It is not uncommon for multiple therapeutics targeting the same proteins to be approved in close succession. In the case of CDK4/6 inhibitors, palbociclib, ribociclib, and abemaciclib have all proven highly effective in the treatment of HR+ metastatic breast cancer and are currently being tested in ~100 ongoing clinical trials for activity in other malignancies. It has hitherto been assumed that the mechanisms of action of the three drugs are very similar, and distinct from those of older-generation CDK inhibitors such as alvocidib: observed differences in the efficacy and toxicity of palbociclib, ribociclib, and abemaciclib have generally been attributed to differences in dosing schedules or potency against CDK4 versus CDK6 (Sherr et al., 2016). However, our work presents six lines of evidence that alvocidib, abemaciclib, palbociclib, and ribociclib actually span a spectrum of increasing selectivity for CDK4/6-cyclin complexes. In particular, abemaciclib has biochemical and physiological activities not manifest by ribociclib and only weakly by palbociclib.

First, exposure of breast cancer cells of different subtypes to any of the three approved CDK4/6 inhibitors induces transcriptional changes associated with G1 arrest but abemaciclib alone induces dose-dependent transcriptional changes similar to those elicited by alvocidib reflective of pan-CDK inhibition. Second, exposing cells to abemaciclib results in more extensive changes in the phosphoproteome than exposure to palbociclib and kinase inference suggests that this is due in part to inhibition of CDK1 and CDK2. Third, kinome profiling using industry-standard KINOMEscan panels, multiplexed inhibitor bead mass spectrometry, and kinase activity assays confirms that abemaciclib has multiple targets in addition to CDK4/6. Fourth, abemaciclib causes arrest of cells in both the G1 and G2 phases of the cell cycle and the drug is cytotoxic (at high concentrations) even in the absence of pRb; in contrast, cells exposed to palbociclib and ribociclib arrest only in G1 and elicit little or no cell death. The difference in efficacy between abemaciclib and other CDK4/6 inhibitors is greatest in cell lines with a transcriptional profile combining higher CCNE1, CDKN1A and CDKL5 and lower CDK9 expression levels. Fifth, in a mouse xenograft model, abemaciclib induces both CDK4/6-like G1 arrest and pan-CDK transcriptional signatures, as observed in cultured cells. Sixth, whereas abemaciclib durably inhibits cell division, cultured cells adapt within 2–3 days of continuous exposure to palbociclib or ribociclib and resume proliferation. Preliminary evidence of the clinical significance of these findings is provided by an abemaciclib-sensitive, palbociclib- and ribociclib-resistant cell line from a deceased patient with HR+/Her2- breast cancer who had progressed on ribociclib/letrozole and by a patient currently responding to abemaciclib as a single agent who had progressed on palbociclib/fulvestrant.

Evidence of substantial differences among CDK4/6 inhibitors is scattered throughout the literature but has not been consolidated or rigorously evaluated, consistent with a general lack of comparative biochemical data on many FDA-approved drugs. Large-scale kinase profiling studies using KINOMEscan, KiNativ, or MIB/MS are one exception to this generalization (Cousins et al., 2017; Fabian et al., 2005; Gelbert et al., 2014; Klaeger et al., 2017; Nomanbhoy et al., 2016). However, our findings strongly argue for a multi-faceted approach to comparative mechanism of action studies. Proteomic, transcriptional, biochemical, and phenotypic approaches measure different aspects of drug action and, in the

current work, a combination of methods was needed to obtain an accurate and complete picture of target spectrum. For example, the false negative finding in KINOMEscan data that abemaciclib does not interact with CDK2 may explain why biological differences among CDK4/6 inhibitors have not been widely appreciated. Similarly, whereas GSK3β was found to be an abemaciclib target of borderline significance by phosphoproteome profiling (perhaps as a result of proteome under-sampling (Riley and Coon, 2016)), it was clearly a target by kinase activity assays (Cousins et al., 2017). Conversely, proteomic profiling assays suggesting that abemaciclib exposure results in down-regulation of AURKA/B and PLK1 activities is most likely an indirect consequence of cell cycle arrest. However, down-regulation of AURKA in particular has been associated with drug sensitivity in general, and may serve as a marker for the responsiveness of MCF7 cells to CDK4/6 inhibition (Donnella et al., 2018). In agreement with Cousins et al. (Cousins et al., 2017), our results using multiple different assays provide little support for the assertion that ribociclib, palbociclib or abemaciclib are systematically more active against CDK4 than CDK6 (Gelbert et al., 2014; Patnaik et al., 2016a, 2016b). Although, enzymatic assays show the IC_{50} for CDK4 is about 2.5-fold greater than for CDK6 for all three drugs, this is unlikely to be therapeutically significant because both targets are strongly inhibited at doses used in patients.

In the case of a polyselective drug such as abemaciclib the question arises whether activities observed at different drug concentrations are all biologically relevant. There is no question that CDK4 and CDK6 are the highest affinity targets of abemaciclib and that abemaciclib is the most potent of the three approved drugs against these CDKs. Our data show abemaciclib to be 10- to 100-fold less potent against CDK2 and CDK1 than CDK4/6, but we detect the cellular consequences of CDK1/2 inhibition in cell lines at concentrations as low as 0.3 μM, well within the C_{max} range in humans, and also achievable in xenograft mouse models (Burke et al., 2016; Patnaik et al., 2016a; Raub et al., 2015). Abemaciclib also exhibits substantially reduced drug adaptation with respect to anti-proliferative effects, which is beneficial for an anti-cancer drug.

The current generation of CDK4/6 inhibitors has benefited from a considerable investment in increasing target selectivity, mainly as a means of reducing toxicity relative to earlier generation drugs (Asghar et al., 2015; Peplow, 2017; Toogood et al., 2005). However, our findings suggest that abemaciclib is not equivalent to palbociclib or ribociclib. Its activities against kinases other than CDK4/6 may be beneficial for anti-cancer activity and targeting them jointly with CDK4/6 may be a means to achieve more durable responses than with CDK4/6 inhibition alone. Inhibition of CDK1/7/9 may also contribute to cell killing (Kitada et al., 2000; Wittmann et al., 2003) and inhibition of mitotic kinases such as TTK may enhance tumor immunogenicity, a key contributor to drug response (Luen et al., 2016). Blocking CDK2/cyclin E should mitigate resistance resulting from amplification of cyclin E (a resistance mechanism in cell culture (Dean et al., 2010; Herrera-Abreu et al., 2016)) and also achieve a more complete therapeutic response by targeting mitotic cells with high CDK2 activity (Asghar et al., 2017). Patients whose tumors exhibit high expression levels of cyclin E1 and are non-responsive to palbociclib (Turner et al., 2019) may thus represent a cohort who might still benefit from treatment with abemaciclib.

STAR Methods

CONTACT FOR REAGENT AND RESOURCE SHARING

Further information and requests for resources and reagents should be directed to and will be fulfilled by the Lead Contact, Peter Sorger (peter_sorger@hms.harvard.edu).

EXPERIMENTAL MODEL AND SUBJECT DETAILS

Cell lines—All cell lines used in this study were of female human breast cancer origin except the MCF 10A and HME1 cell lines that were derived from non-transformed human breast epithelia. Cell lines were maintained, free of mycoplasma, in their recommended growth conditions listed below, and were identity-validated by STR profiling (Reid et al., 2004).

Cell line	Growth media	Growth conditions
BT20	EMEM + 10% FBS + 1% P/S	37°C, 5% CO2
BT549	RPMI-1640 + 10% FBS + 1% P/S, 1 ug/ml IN	37°C, 5% CO2
CAL120	DMEM + 10% FBS + 1% P/S	37°C, 5% CO2
CAL51	DMEM + 20% FBS + 1% P/S	37°C, 5% CO2
CAL851	DMEM + 10% FBS + 1% P/S	37°C, 5% CO2
CAMA1	EMEM + 10% FBS + 1% P/S	37°C, 5% CO2
HCC1143	RPMI-1640 + 10% FBS + 1% P/S	37°C, 5% CO2
HCC1395	RPMI-1640 + 10% FBS + 1% P/S	37°C, 5% CO2
HCC1419	RPMI-1640 + 10% FBS + 1% P/S	37°C, 5% CO2
HCC1428	RPMI-1640 + 10% FBS + 1% P/S	37°C, 5% CO2
HCC1500	RPMI-1640 + 10% FBS + 1% P/S	37°C, 5% CO2
HCC1806	RPMI-1640 + 10% FBS + 1% P/S	37°C, 5% CO2
HCC1937	RPMI-1640 + 10% FBS + 1% P/S	37°C, 5% CO2
HCC1954	RPMI-1640 + 10% FBS + 1% P/S	37°C, 5% CO2
HCC38	RPMI-1640 + 10% FBS + 1% P/S	37°C, 5% CO2
HCC70	RPMI-1640 + 10% FBS + 1% P/S	37°C, 5% CO2
HME1	MEMB + Lonza CC-3150 kit	37°C, 5% CO2
HS578T	DMEM + 10% FBS + 1% P/S	37°C, 5% CO2
MCF10A	DMEM/F12 (1:1) + 5% HS + 1% P/S, 20ng/ml EGF, 0.5mg/ml HC, 10 ug/ml IN, 100ng/ml CT	37°C, 5% CO2
MCF7	DMEM + 10% FBS + 1% P/S	37°C, 5% CO2
MDAMB157	L-15 + 10% FBS + 1% P/S	37°C, no CO2
MDAMB231	DMEM + 10% FBS + 1% P/S	37°C, 5% CO2
MDAMB361	L-15 + 20% FBS + 1% P/S	37°C, no CO2
MDAMB436	L-15 + 10% FBS + 1% P/S, 10ug/ml IN	37°C, no CO2
MDAMB453	L-15 + 10% FBS + 1% P/S	37°C, no CO2
MDAMB468	L-15 + 10% FBS + 1% P/S	37°C, no CO2

Cell line	Growth media	Growth conditions
MGH312	RPMI-1640 + 10% FBS + 1% P/S	37°C, 5% CO2
PDX1258	DMEM/F12 (3:1) + 7.5% FBS + 1% P/S, 0.125ng/ml EGF, 25ng/ml HC, 5ug/ml IN, 8.6ng/ml CT, 5 uM Y-27632 (Palechor-Ceron et al., 2013)	37°C, 5% CO2
PDX1328	DMEM/F12 (3:1) + 7.5% FBS + 1% P/S, 0.125ng/ml EGF, 25ng/ml HC, 5ug/ml IN, 8.6ng/ml CT, 5 uM Y-27632 (Palechor-Ceron et al., 2013)	37°C, 5% CO2
PDXHCI002	DMEM/F12 (3:1) + 7.5% FBS + 1% P/S, 0.125ng/ml EGF, 25ng/ml HC, 5ug/ml IN, 8.6ng/ml CT, 5 uM Y-27632 (Palechor-Ceron et al., 2013)	37°C, 5% CO2
SKBR3	McCoy's + 10% FBS + 1% P/S	37°C, 5% CO2
SUM1315	F-12 + 5% FBS + 1% P/S, 10ng/ml EGF, 5ug/ml IN, 10mM HEPES	37°C, 5% CO2
SUM149	F-12 + 5% FBS + 1% P/S, 1ug/ml HC, 5ug/ml IN, 10mM HEPES	37°C, 5% CO2
SUM159	F-12 + 5% FBS + 1% P/S, 1ug/ml HC, 5ug/ml IN, 10mM HEPES	37°C, 5% CO2
T47D	RPMI-1640 + 10% FBS + 1% P/S, 1 ug/ml IN	37°C, 5% CO2

Abbreviations: fetal bovine serum (FBS), penicillin/streptomycin (P/S), insulin (IN), hydrocortisone (HC), epidermal growth factor (EGF), cholera toxin (CT). Reagent details can be found in the Key Resources Table.

Animals—Seven-week-old female NU/NU nude (Crl:NU-Foxn1[nu]) mice (RRID IMSR_CRL:088) were used for this study (Charles River, Wilmington, MA). The animals were housed five per cage in the Harvard Center for Comparative Medicine animal facility and had *ad libitum* access to food and water (supplemented with 8 μg/ml 17 ß-estradiol to sustain growth of the hormone receptor positive xenografted tumor cells). Once tumors reached 250 mm^3 the mice were randomly assigned to treatment groups. All animal experiments were conducted in accordance with protocols approved by the Institutional Animal Care and Use Committee (IACUC) at Harvard Medical School.

METHOD DETAILS

Dose response measurements—Cells were plated at densities ranging from 500 to 2000 cells per well in 384-well Cell Carrier plates (Perkin Elmer, Waltham, MA) using a Multidrop Combi Reagent Dispenser (Thermo Fisher Scientific, Waltham, MA) and grown for 36 hours. Cells were treated with a dilution series of the indicated drugs by pin transfer or using a D300 Digital Dispenser (Hewlett-Packard, Palo Alto, CA). Drugs were obtained from commercial vendors and tested for purity in-house as described in detail in the HMS LINCS drug collection database (http://lincs.hms.harvard.edu/db/sm/). Cells were stained and fixed for analysis at the time of drug delivery and after 24 to 144 hours of incubation depending on the experiment. Cells were stained at the indicated time points with 2 μg/ml Hoechst 33342 (Sigma Aldrich, St. Louis, MO) and 1:1000 LIVE/DEAD Far Red Dead Cell Stain (Thermo Fisher Scientific, Waltham, MA) for 30 minutes and fixed with 3.7% formaldehyde (Sigma Aldrich, St. Louis, MO) for 30 minutes. Fixed cells were imaged with a 10x objective using an Operetta microscope and analyzed using the Columbus image data storage and analysis system (Perkin Elmer, Waltham, MA). For most experiments, each condition was tested across three replicate plates and at least four wells per cell line per plate were untreated.

Nuclei counts were normalized to DMSO-treated controls on the same plate to yield relative cell count and normalized growth rate inhibition (GR) values for each technical replicate for

each condition (Hafner et al., 2016). Technical replicates were averaged to yield mean relative cell counts and the mean GR value for each condition within each biological replicate. Within each biological replicate, mean GR values for a given cell line /small molecule combination across all tested concentrations were fitted to a biphasic sigmoidal curve with the equation:

$$GR(c) = 2^{\log_2\left(GR_{max}^{1st} + \frac{1 - GR_{max}^{1st}}{1 + \left(c/GEC_{50}^{1st}\right)^{h^{1st}}} + 1\right) \cdot \log_2\left(GR_{max}^{2nd} + \frac{1 - GR_{max}^{2nd}}{1 + \left(c/GEC_{50}^{2nd}\right)^{h^{2nd}}} + 1\right)} - 1,$$

or with a single sigmoidal curve with the equation:

$$GR(c) = GR_{max} + \frac{1 - GR_{max}}{1 + \left(c/GEC_{50}\right)^{h}} + 1,$$

or with a flat line with the equation $GR(c) \equiv GR_{max}$. The significance of each curve was assessed using an F-test and the most complex model with $P < 0.05$ was considered to best fit the data. The parameters of the sigmoidal curve and the first phase of the biphasic curve are constrained as described in Hafner et al. (Hafner et al., 2017b). In the biphasic curve, the parameter GEC_{50}^{2nd} is constrained to be above 0.3 μM. The time-dependent GR values (Hafner et al., 2016) for Figure 7a were evaluated over a 48-hour interval.

Phospho-pRb immunofluorescence and cell cycle analysis—Cells were seeded in 384-well plates, allowed to adhere for 24–36 hours, treated with CDK4/6 inhibitors, incubated for the desired amount of time then fixed in 4% formaldehyde, permeabilized with 0.5% Triton X-100 in PBS, and blocked with Odyssey blocking buffer (LI-COR, Lincoln, NE). Cells were labeled overnight at 4°C with a 1:800 dilution of anti-phospho-pRb Alexa-555 (Ser807/811) (Cell Signaling Technologies, Danvers, MA) and 2 μg/ml Hoechst 33342 (Sigma Aldrich, St. Louis, MO) prepared in Odyssey blocking buffer. Images were acquired with a Perkin Elmer Operetta microscope as described for the dose response measurements. Nuclei were segmented using Columbus software (Perkin Elmer, Waltham, MA) based on their Hoechst signal. DNA content was defined by the total Hoechst intensity within the nuclear mask. The average phospho-pRb intensity within the nuclear mask was determined, and a threshold for positivity was set by visually inspecting images of several control and treated wells per cell line. For more detailed cell cycle analysis, cells were labeled with a Click-iT™ EdU Alexa Fluor™ 488 Imaging Kit according to the manufacturer's directions (one hour EdU pulse prior to fixation) (Thermo Fisher Scientific, Waltham, MA). Imaging and segmentation were the same as for the immunofluorescence experiments. The average EdU intensity within the nuclear mask was determined. DNA content was used to identify cells in the G1 and G2 phases of the cell cycle, EdU intensity was used to identify cell in S phase. Cells with no EdU signal, and intermediate DNA content were classified as S-phase dropout cells.

mRNA-seq—Cells were seeded in 12-well plates, and allowed to adhere for 24 hours at which time CDK4/6 inhibitors were added. Cells were lysed in the plates after 6 or 24 hours, and RNA was extracted using Applied Biosystems MagMax 96 total RNA isolation kit (Thermo Fisher Scientific, Waltham, MA) with DNAse digestion according to the manufacturer's protocol. RNA was checked for quantity with a NanoDrop (Thermo Fisher Scientific, Waltham, MA) and for quality using an Agilent Bioanalyzer instrument (with RIN value > 9.0). Libraries were prepared using a TruSeq Stranded mRNA sample preparation kit (Illumina, San Diego, CA) from 500 ng of purified total RNA according to the manufacturer's protocol in a reduced reaction volume. The finished cDNA libraries were assessed for quality using a Bioanalyzer and quantified with a Quant-iT dsDNA Assay kit (Thermo Fisher Scientific, Waltham, MA). The uniquely indexed libraries were multiplexed based on this quantitation and the pooled sample was quantified by qPCR using the Kapa Biosystems (Wilmington, MA) library quantification kit by the Molecular Biology Core Genomics Facility at the Dana-Farber Cancer Institute and sequenced on a single Illumina NextSeq500 run with single-end 75bp reads.

Reads were processed to counts using the bcbio-Nextgen toolkit version 1.0.3a (https://github.com/chapmanb/bcbio-nextgen) as follows: (1) Reads were trimmed and clipped for quality control in cutadapt v1.12; (2) Read quality was checked for each sample using FastQC 0.11.5; (3) High-quality reads were then aligned into BAM files through STAR 2.5.3a using the human assembly GRCh37; (4) BAM files were imported into DEXSeq-COUNT 1.14.2 and raw counts TPM and RPKM were calculated. R package edgeR (McCarthy et al., 2012; Robinson et al., 2010) 3.18.1 (R version 3.2.1) was used for differential analysis and generate log fold change, *P*-value and FDR.

3'DGE sequencing—Cells were plated at densities ranging from 500 to 2000 cells per well in a 384-well Cell Carrier plate (Perkin Elmer, Waltham, MA) and allowed to adhere for 24 hours. Cells were treated with the CDK4/6 inhibitors, alvocidib, or DMSO using a D300 Digital Dispenser (Hewlett-Packard, Palo Alto, CA). After six hours, the cells were washed once with PBS using an EL405x plate washer (BioTek, Winooski, VT), 10 μl of 1X TCL lysis buffer with 1% (v/v) ß-mercaptoethanol (Qiagen, Hilden, Germany) was added per well, and the plates were stored at −80˚C until the RNA extraction was performed. For RNA extraction, the cell lysate plate was thawed, vortexed briefly, and centrifuged for 1 min at 1000 rpm. Using a BRAVO (Agilent, Santa Clara, CA) liquid handler, the lysate was mixed thoroughly before transferring 10 μl to a 384 well PCR plate. 28 μl of SPRI beads (Beckman Coulter Genomics, Chaska, MN) were added directly to the lysate, mixed and incubated for 5 min. The plate was transferred to a magnetic rack to aggregate the beads, and incubated for 5 min prior to removing the liquid. The beads were washed with 80% ethanol twice, allowed to dry for 1 min, 20 μl of nuclease free water was added per well, the plate was removed from the magnetic rack and the beads were thoroughly resuspended. Following a 5 min incubation, the plate was returned to the magnetic rack and incubated an additional 5 min before transferring the supernatant to a fresh PCR plate. 5 μl of the supernatant was transferred to a separate plate containing RT master mix and 3' and 5' adapters for reverse transcription and template switching (Soumillon et al., 2014), and incubated for 90 min at 42˚C. The cDNA was pooled and purified with a QIAquick PCR purification kit according

to the manufacturer's directions with the final elution in 24 μl of nuclease free water. This was followed by an exonuclease I treatment for 30 min at 37˚C that was stopped with a 20 min incubation at 80˚C. The cDNA was then amplified using the Advantage 2 PCR Enzyme System (Takara, Fremont, CA) for 5 cycles, and purified using AMPure XP magnetic beads (Beckman Coulter Genomics, Chaska, MN). Library preparation was completed with 55 ng input using a Nextera DNA kit (Illumina, San Diego, CA) following the manufacturer's instructions, amplified 5 cycles, and purified with AMPure XP magnetic beads (Beckman Coulter Genomics, Chaska, MN). A Pippin PREP purification of the sample from 300–800bp was performed, it was then quantified by qPCR and sequenced on a single Illumina NextSeq run with 75bp paired end reads at the Harvard University Bauer Core Facility.

Reads were processed to counts through the bcbio-nextgen single cell/DGE RNA-seq analysis pipeline (https://bcbio-nextgen.readthedocs.io/en/latest/contents/pipelines.html) a brief description follows: The well barcode and UMIs were identified for all reads and all reads not within one edit distance of a known well barcode were discarded. Each surviving read was quasialigned to the transcriptome (GRCh38) using RapMap (Srivastava et al., 2016). Reads per well were counted using UMIs (Svensson et al., 2017), discarding duplicated UMIs, weighting multimapped reads by the number of transcripts they aligned to and collapsing counts to genes by adding all counts for each transcript of a gene. The R package edgeR 3.18.1 (R version 3.2.1) was used for differential expression analysis.

Clustering analysis of the mRNA-seq data and L1000 signatures—Differential gene expression signatures were clustered along samples and genes based on the cosine distance for the $\log_2$(fold-change) using MATLAB default functions. $\log_2$(fold-change) values for genes with FDR values above 0.2 were set to zero. In Figure 1a, the two down-regulated gene clusters were defined manually based on the dendrogram of the genes. The 'LINCS_L1000_Chem_Pert_down' library obtained from Enrichr (Kuleshov et al., 2016) was used as the reference signature of genes down-regulated upon drug perturbation (Table S1). Enrichment analysis was performed on the two down-regulated gene clusters (Figure 1a) against the reference library using the GSEA algorithm (gsea2–2.2.3.jar from the Broad Institute (Subramanian et al., 2005)). Enrichment scores for 31 well-annotated drugs that feature in the library were reported (Figure 1b–c) as $-\log_{10}(P$-value). G1-arrest and pan-CDK scores for each condition (Figure S1, Figure 1d) were computed as the mean $\log_2$(fold-change) across the genes in the red (G1-arrest) and cyan (pan-CDK) down-regulated gene clusters identified in Fig 1a. G1-arrest and pan-CDK scores for 3' DGEseq (Figure 2) and MCF7-xenograft mRNAseq (Figure 6b) were computed on the same set of down-regulated genes.

Phosphoproteomics mass spectrometry—MCF7 cells were treated with 0.3 μM or 3 μM palbociclib or abemacicblib, or DMSO control for 1 hour in duplicate. For each sample, 4.5 mg of protein was utilized to perform serine and threonine phosphoproteome analysis. The samples were digested using Trypsin (Promega, Madison, WI), acidified and desalted using C18 Sep-Pak (Waters, Milford, MA). Phosphopeptides were enriched using the Thermo Scientific High-Select Fe-NTA Phosphopeptide Enrichment Kit. The samples were labeled using a TMT 10plex Mass Tag Labeling kit (Thermo Fisher Scientific, Waltham,

MA) and the reaction was quenched by adding hydroxylamine to a final concentration of 0.5% (v/v) (Kettenbach and Gerber, 2011; Paulo et al., 2015). The sample was then enriched for phosphotyrosine-containing peptides using the pY-1000 antibody (Cell Signaling Technologies, Danvers, MA) coupled to Pierce Protein A Agarose beads (Thermo Fisher Scientific, Waltham, MA). The flow-through from the pY sample was kept and desalted for pS and pT analysis. 24 fractions (phosphoproteomics) were then desalted using the C18 StageTip procedure (Rappsilber et al., 2007). All MS analyses were performed on an Orbitrap Fusion Lumos mass spectrometer (Thermo Fisher Scientific, Waltham, MA) using a multi-notch MS3 method (McAlister et al., 2014; Ting et al., 2011). Raw data were converted to mzXML and searched via Sequest (Eng et al., 1994) version 28 against a concatenated Uniprot database (downloaded 02/04/2014). Linear discriminate analysis was used to distinguish forward and reverse hits and reverse hits were filtered to an FDR of 1% at the protein level. Site localization confidence was assessed using the A-score method (Beausoleil et al., 2006). Reporter ion intensities were quantified and normalized as described earlier (Paulo et al., 2015).

Annotation of phosphopeptides with upstream kinases—16,300 phosphopeptides were detected across all conditions in MCF7 cells. The PhosphoSitePlus (PSP) database (Hornbeck et al., 2012), which contains curated annotations of upstream kinases, was queried using phosphopeptide sequence motifs and UniProt IDs as identifiers. Only ~6.3% of the phosphopeptides detected by phosphoproteomics had experimentally verifiable kinase annotations on PSP. The NetworKIN algorithm (Horn et al., 2014) that predicts upstream kinases, based on phosphopeptide sequences and STRING evidence, was used to identify kinases for the remaining phosphosites. A further 14% of phosphosites were annotated with predicted kinases (NetworKIN Score > 4). In total, 3145 phosphopeptides from 1242 proteins were annotated as being phosphorylated by 365 kinases (8297 kinase-peptide interaction pairs).

Differential kinase activity score using GSEA—Based on the method described previously (Drake et al., 2012), a custom python package was developed to infer differential kinase activity across drug treatments (https://github.com/datarail/msda). A kinase set library was assembled using the identified kinase-substrate relationships. The kinase set library is composed of kinases and their corresponding sets of phosphopeptide substrates. Only kinase sets that had more than 25 downstream phosphosites were used. The final kinase set library was composed of 60 kinases that phosphorylate 2597 peptides. For each phosphopeptide, the mean difference between the replicates and the maximum difference across conditions were computed. If the delta between the two scores was less than 1, then the phosphopeptide measurement was considered noisy and discarded, resulting in a final list of 9958 phosphopeptides (Table S2). For each of the four treatment conditions, the average $\log_2$(fold-change) was computed relative to the untreated control. Using the phosphopeptide $\log_2$(fold-change) values as input and the final kinase set library, GSEA algorithm (gsea2–2.2.3.jar from Broad Institute (Subramanian et al., 2005)) was used to infer the enrichment score ($P < 0.05$ and FDR < 0.2). The enrichment score is a proxy metric for the differential activity of the kinases.

Measurement of kinase inhibition with kinobeads—Multiplex inhibitor beads (MIB) (Duncan et al., 2012) were generously provided by Gary Johnson (University of North Carolina). A mixed cell lysate comprised of K562, COLO0205, SK-N-BE(2), MV-4–11 cells was prepared as previously described (Médard et al., 2015), and clarified by filtration through 0.45 μm and 0.22 μm filters. 3 mg of the mixed cell lysate was treated with CDK4/6 inhibitors or DMSO overnight at 4°C with continuous rocking. The samples were enriched for kinases by passing them through a sepharose bead column followed by a MIB column. The samples were washed with MIB wash buffer (50 mM HEPES pH 7.5, 0.5% Triton X-100, 1 mM EDTA, 1 mM EGTA) with high (1 M NaCl) and low (150 mM NaCl) salt, and then in low salt MIB buffer containing 0.1% SDS (w/v). Kinases bound to the MIBs were eluted twice with 500 μl/column of MIB elution buffer (0.5% (w/v) SDS, 10 μM DTT, 0.1 M Tris-HCl pH 6.8). The eluent was boiled for 15 min at 97°C, and alkylated with 0.5 M iodoactamide (30 μl per ml of sample) for 30 min at room temperature. The samples were precipitated with tricholoracetic acid (25% final volume), washed twice with methanol, and dried. The samples were solubilized in 8 M urea in 20 mM EPPS. Additional EPPS was added to decrease the concentration of urea to 2 M prior to adding acetonitrile (ACN) and lysC (2 μg/μl) for 3 hours at room temperature. The samples were digested with trypsin (0.5 μg/μl) overnight at 37°C. Additional ACN was added, followed by 5 μl of tandem mass tag (TMT) labels (Thermo Fisher Scientific, Waltham, MA) for 1 hour at room temperature. At this stage a ratio check was performed to ensure equal loading of each individually TMT-labeled sample, and to check the efficiency of the labeling reaction. The labeling reactions were quenched with 5 μl of 10% hydroxylamine for 10 min at room temperature, at which point the samples were pooled, diluted with 100% formic acid, evaporated to 0.5 ml, diluted with 1% formic acid, and then desalted by passing through a solid phase extraction cartridge (Thermo Fisher Scientific, Waltham, MA). Samples were eluted in 70% ACN and 1% formic acid, evaporated, and reconstituted in 300 μl of 0.1% TFA. The samples were analyzed on an Orbitrap Fusion Lumos mass spectrometer. Peptide intensities of the proteins pulled down by the MIBs were summed to obtain total protein intensities. The protein intensities were normalized using the iBAQ method (Schwanhäusser et al., 2011). For each treatment condition, log2(fold-change) values were computed relative to untreated (DMSO) control.

***In vitro* measurement of kinase inhibitory activity—**Ribociclib, palbociclib, and abemaciclib were assayed using the KINOMEscan® assay platform (DiscoverX, Fremont, CA). Data are reported as percent of remaining activity at either 0.1 or 1.0 μM drug concentration. The activity of ribociclib, palbociclib, abemaciclib, and alvocidib on multiple CDK-cyclin complexes and other kinases were assayed using Thermo Fisher Scientific SelectScreen Kinase Profiling service. The 'Adapta™' assay was used for CDK4/cyclin D1, CDK4/cyclin D3, CDK6/cyclin D1, CDK7/cyclin H/MNAT1, and CDK9/cyclin T1. The 'LanthaScreen™' Kinase Binding assay was used for CDK2/cyclin A1, CDK2/cyclin E1, CDK9/cyclin K, and TTK. The 'Z′-LYTE™' assay was used for CDK1/cyclin B, AURKA, AURKB, CAMK2A, GSK3B, and PLK1. The ATP concentration was Km[app] when available or 10 μM otherwise. The activities of ribociclib, palbociclib, and abemaciclib on CDK4 and CDK6 complexes with cyclins D1 and D3 were assayed using Reaction Biology

Corporation's (Malvern, PA) Kinase Profiling services as described (Anastassiadis et al., 2011). The ATP concentration was 10 μM.

Western blots—20 μg of whole cell lysate (Figure 7b) or 12 μg of whole cell lysate (Figure S7), prepared in M-PER lysis buffer (Thermo Fisher Scientific, Waltham, MA) with complete protease inhibitor cocktail (Sigma Aldrich, St. Louis, MO), was added per well in Mini-PROTEAN TGX precast gels (Bio-Rad, Hercules, CA). Primary mouse monoclonal pRb, cyclin E, and β-actin antibodies were used at 1:1000 dilutions. Secondary anti-mouse IgG, HRP-linked was used 1:2000. All antibodies were from Cell Signaling Technologies (Danvers, MA).

Immunohistochemistry—A 4 μm slice of a formalin-fixed, paraffin-embedded, biopsy of the liver lesion from which the MGH312 cell line was derived (Crystal et al., 2014) was mounted on a standard glass slide and stained for RB expression using a Leica Bond autostainer. The primary Rb antibody (clone 1F8; Bio SB, Santa Barbara, CA) was diluted 1:500 in Leica Bond Diluent and incubated for 15 min. The slide was counterstained with hematoxylin.

Identifying genes associated with differential efficacy of abemaciclib and palbociclib—We selected 30 genes related to the cell cycle (cyclins, CDKs, CDKLs, and CDKNs), whether or not they are known CDK4/6 inhibitor on- or off-targets. Using the baseline mRNA expression of these genes, we built a multilinear model (MATLAB function 'fitglm') to predict the difference in GR values at 3.16 μM between palbociclib and abemaciclib for the pRb-proficient cell lines profiled in Figure 4a. Predictors with non-significant coefficients ($P > 0.05$) were iteratively removed until only significant coefficients remained. A leave-one-out cross validation was performed with the remaining predictors to yield the results in Figure 4c. Note that results were qualitatively similar if the pRb-deficient cell lines were included.

In vivo studies—Thirty-five seven-week-old NU/NU nude mice (Charles River Laboratories, Wilmington, MA) were supplemented with 8 μg/ml 17ß-estradiol (Sigma Aldrich, St. Louis, MO) by adding it to their drinking water five days prior to tumor engraftment, and replacing it twice per week. Mice were engrafted with 5×10^6 MCF-7 cells 1:1 in growth factor reduced matrigel (Corning, Corning, NY) subcutaneously in each flank, and allowed to grow to ~250 mm^3. The animals were then randomly assigned to treatment groups, and treated daily for four days with ribociclib (150 mg/kg), palbociclib (150 mg/kg), abemaciclib (25, 75, 100, 125, or 150 mg/kg), or vehicle control (0.5% (w/v) hydroxyethyl cellulose (Sigma Aldrich, St. Louis, MO) and 0.05% (v/v) antifoam (Sigma Aldrich, St. Louis, MO) in water) by oral gavage. Animals were sacrificed two hours after receiving the last dose. The tumors were excised and cut in half, one half was fixed in 4% formaldehyde at 4°C and transferred to 0.1% sodium azide after 48 hours, the other flash frozen, and a thin slice from the center of the tumor was placed in RNA*later* at 4°C (Qiagen, Hilden, Germany), after 48 hours the RNA*later* was aspirated, and samples were transferred to −80°C.

The fixed tumor samples were paraffin-embedded at the Harvard Medical Area Rodent Histopathology Core and a tissue microarray (TMA) was constructed at the Tissue Microarray & Imaging Core by arraying three 1 mm cores per sample in a block. Sequential 5 μm slices were mounted on superfrost slides. The slides were subjected to manual dewaxing and antigen retrieval as described previously (Lin et al., 2017). The slides were then blocked with Odyssey buffer (LI-COR, Lincoln, NE) and pre-stained with secondary antibodies prior to beginning cyclic immunofluorescence (Lin et al., 2017). The antibodies used in this study are listed in the Key Resources Table. Images were acquired on a RareCyte CyteFinder (Seattle, WA) slide scanning microscope with a 10X 0.3 NA objective. Image quantitation was performed in ImageJ as previously described (Lin et al., 2017). Human cells were distinguished from mouse cells based on e-cadherin and vimentin intensities, and only the e-cadherin-high, vimentin-low cells were included in subsequent analyses. A threshold for phospho-pRb positive cells was set manually by comparing the intensity distributions of phospho-pRb staining in tumors from mice that received the vehicle control and 150 mg/kg palbociclib.

The RNA*later* preserved samples were thawed on ice, 600 μl of RLT with 10% 2-mercaptoethanol was added and the tumors were manually dissociated with microfuge pestles (Thomas Scientific, Swedesboro, NJ). Samples were passed through QiaShredder columns, and then loaded on RNeasy columns (Qiagen, Hilden, Germany) and processed according to the manufacturer's specifications with a 30 min incubation in DNase. Library preparation, and analysis were performed as described in section 4. A single Illumina NextSeq500 run with single-end 75bp reads was performed at the Harvard Medical School Biopolymers Facility. Reads were processed as described in section 4, with the additional step that the alignment algorithm identified and excluded reads that aligned with the mouse genome to ensure that downstream analyses were performed on the xenograft transcripts only. Non-coding genes were excluded from the transcript per million (TPM) counts table and Principal Component Analyses (PCA) was performed. For each treated sample, the fold-change of transcripts relative to vehicle control was computed using edgeR (Robinson et al., 2010). G1 and pan-CDK scores were computed as described in section 6.

QUANTIFICATION AND STATISTICAL ANALYSIS

Image quantification was performed with Columbus (Perkin Elmer, Waltham, MA) software. All subsequent analyses were performed using MATLAB and python. All relevant statistical details are included in the figure captions, and text. Additional details for each experiment type are included in the METHOD DETAILS section of the STAR Methods.

DATA AND SOFTWARE AVAILABILITY

The RNA sequencing data sets related to Figures 1, 2, and 6 have been deposited on GEO, and can be found under accession numbers GSE99116, GSE125215 and GSE124854 respectively. The phosphoproteomics data set related to Figure 3 is freely available on Synapse, ID syn18488089, https://www.synapse.org/#!Synapse:syn18488089. The dose response data sets related to Figure 4 are available in the HMS LINCS database, IDs 20343

and 20344, http://lincs.hms.harvard.edu/db/datasets/20343/ http://lincs.hms.harvard.edu/db/datasets/20344/.

All supplemental data can be freely accessed through Synapse, ID syn18488085, https://www.synapse.org/#!Synapse:syn18488085/wiki/590635 and via the HMS LINCS page https://lincs.hms.harvard.edu/hafner-mills-etal-2019/.

Supplementary Material

Refer to Web version on PubMed Central for supplementary material.

REFERENCES

Anastassiadis T, Deacon SW, Devarajan K, Ma H, and Peterson JR (2011). Comprehensive assay of kinase catalytic activity reveals features of kinase inhibitor selectivity. Nat. Biotechnol 29, 1039–1045. [PubMed: 22037377]

Asghar U, Witkiewicz AK, Turner NC, and Knudsen ES (2015). The history and future of targeting cyclin-dependent kinases in cancer therapy. Nat. Rev. Drug Discov 14, 130–146. [PubMed: 25633797]

Asghar U, Barr AR, Cutts R, Beaney M, Babina I, Sampath D, Giltnane J, Lacap JA, Crocker L, Young A, et al. (2017). Single-Cell Dynamics Determines Response to CDK4/6 Inhibition in Triple-Negative Breast Cancer. Clin. Cancer Res. Off. J. Am. Assoc. Cancer Res 23, 5561–5572.

Balko JM, Giltnane JM, Wang K, Schwarz LJ, Young CD, Cook RS, Owens P, Sanders ME, Kuba MG, Sánchez V, et al. (2014). Molecular profiling of the residual disease of triple-negative breast cancers after neoadjuvant chemotherapy identifies actionable therapeutic targets. Cancer Discov 4, 232–245. [PubMed: 24356096]

Beausoleil SA, Villén J, Gerber SA, Rush J, and Gygi SP (2006). A probability-based approach for high-throughput protein phosphorylation analysis and site localization. Nat. Biotechnol 24, 1285–1292. [PubMed: 16964243]

Burke T, Torres R, McNulty A, Dempsey J, Kolis S, Kulanthaivel P, and Beckmann R (2016). Abstract 2830: The major human metabolites of abemaciclib are inhibitors of CDK4 and CDK6. Cancer Res 76, 2830–2830.

Caunt CJ, Sale MJ, Smith PD, and Cook SJ (2015). MEK1 and MEK2 inhibitors and cancer therapy: the long and winding road. Nat. Rev. Cancer 15, 577–592. [PubMed: 26399658]

Chen P, Lee NV, Hu W, Xu M, Ferre RA, Lam H, Bergqvist S, Solowiej J, Diehl W, He Y-A, et al. (2016). Spectrum and Degree of CDK Drug Interactions Predicts Clinical Performance. Mol. Cancer Ther 15, 2273–2281. [PubMed: 27496135]

Cousins EM, Goldfarb D, Yan F, Roques J, Darr D, Johnson GL, and Major MB (2017). Competitive Kinase Enrichment Proteomics Reveals that Abemaciclib Inhibits GSK3β and Activates WNT Signaling. Mol. Cancer Res

Cristofanilli M, Turner NC, Bondarenko I, Ro J, Im S-A, Masuda N, Colleoni M, DeMichele A, Loi S, Verma S, et al. (2016). Fulvestrant plus palbociclib versus fulvestrant plus placebo for treatment of hormone-receptor-positive, HER2-negative metastatic breast cancer that progressed on previous endocrine therapy (PALOMA-3): final analysis of the multicentre, double-blind, phas. Lancet Oncol 17, 425–439. [PubMed: 26947331]

Crystal AS, Shaw AT, Sequist LV, Friboulet L, Niederst MJ, Lockerman EL, Frias RL, Gainor JF, Amzallag A, Greninger P, et al. (2014). Patient-derived models of acquired resistance can identify effective drug combinations for cancer. Science 346, 1480 LP–1486. [PubMed: 25394791]

Dean JL, Thangavel C, McClendon AK, Reed CA, and Knudsen ES (2010). Therapeutic CDK4/6 inhibition in breast cancer: key mechanisms of response and failure. Oncogene 29, 4018–4032. [PubMed: 20473330]

Dickler MN, Tolaney SM, Rugo HS, and Cortes J (2016). MONARCH1: Results from a phase II study of abemaciclib, a CDK4 and CDK6 inhibitor, as monotherapy, in patients with HR+/HER2- breast cancer, after chemotherapy for advanced disease. J Clin Oncol 34 34.

Donnella HJ, Webber JT, Levin RS, Camarda R, Momcilovic O, Bayani N, Shah KN, Korkola JE, Shokat KM, Goga A, et al. (2018). Kinome rewiring reveals AURKA limits PI3K-pathway inhibitor efficacy in breast cancer. Nat. Chem. Biol 14, 768. [PubMed: 29942081]

Drake JM, Graham N. a., Stoyanova T, Sedghi A, Goldstein a. S., Cai H, Smith D. a., Zhang H, Komisopoulou E, Huang J, et al. (2012). Oncogene-specific activation of tyrosine kinase networks during prostate cancer progression. Proc. Natl. Acad. Sci

Duncan JS, Whittle MC, Nakamura K, Abell AN, Midland AA, Zawistowski JS, Johnson NL, Granger DA, Jordan NV, Darr DB, et al. (2012). Dynamic Reprogramming of the Kinome in Response to Targeted MEK Inhibition in Triple-Negative Breast Cancer. Cell 149, 307–321. [PubMed: 22500798]

Echalier A, Hole AJ, Lolli G, Endicott JA, and Noble MEM (2014). An inhibitor's-eye view of the atp-binding site of CDKs in different regulatory states. ACS Chem. Biol 9, 1251–1256. [PubMed: 24669831]

Eng JK, McCormack AL, and Yates JR (1994). An approach to correlate tandem mass spectral data of peptides with amino acid sequences in a protein database. J. Am. Soc. Mass Spectrom 5, 976–989. [PubMed: 24226387]

Fabian MA, Biggs III WH, Treiber DK, Atteridge CE, Azimioara MD, Benedetti MG, Carter TA, Ciceri P, Edeen PT, Floyd M, et al. (2005). A small molecule–kinase interaction map for clinical kinase inhibitors. Nat. Biotechnol 23, 329. [PubMed: 15711537]

Finn RS, Dering J, Conklin D, Kalous O, Cohen DJ, Desai AJ, Ginther C, Atefi M, Chen I, Fowst C, et al. (2009). PD 0332991, a selective cyclin D kinase 4/6 inhibitor, preferentially inhibits proliferation of luminal estrogen receptor-positive human breast cancer cell lines in vitro. Breast Cancer Res. BCR 11, R77. [PubMed: 19874578]

Franco J, Witkiewicz AK, and Knudsen ES (2014). CDK4/6 inhibitors have potent activity in combination with pathway selective therapeutic agents in models of pancreatic cancer. Oncotarget 5, 6512–6525. [PubMed: 25156567]

Fry DW, Harvey PJ, Keller PR, Elliott WL, Meade M, Trachet E, Albassam M, Zheng X, Leopold WR, Pryer NK, et al. (2004). Specific inhibition of cyclin-dependent kinase 4/6 by PD 0332991 and associated antitumor activity in human tumor xenografts. Mol. Cancer Ther 3, 1427 LP–1438. [PubMed: 15542782]

Gelbert LM, Cai S, Lin X, Sanchez-Martinez C, Del Prado M, Lallena MJ, Torres R, Ajamie RT, Wishart GN, Flack RS, et al. (2014). Preclinical characterization of the CDK4/6 inhibitor LY2835219: in-vivo cell cycle-dependent/independent anti-tumor activities alone/in combination with gemcitabine. Invest. New Drugs 32, 825–837. [PubMed: 24919854]

Goel S, Wang Q, Watt AC, Tolaney SM, Dillon DA, Li W, Ramm S, Palmer AC, Yuzugullu H, Varadan V, et al. (2016). Overcoming Therapeutic Resistance in HER2-Positive Breast Cancers with CDK4/6 Inhibitors. Cancer Cell 29, 255–269. [PubMed: 26977878]

Griggs JJ, and Wolff AC (2017). Cyclin-Dependent Kinase 4/6 Inhibitors in the Treatment of Breast Cancer: More Breakthroughs and an Embarrassment of Riches. J. Clin. Oncol. Off. J. Am. Soc. Clin. Oncol. JCO2017739375.

Hafner M, Niepel M, Chung M, and Sorger PK (2016). Growth rate inhibition metrics correct for confounders in measuring sensitivity to cancer drugs. Nat. Methods 13, 521–527. [PubMed: 27135972]

Hafner M, Niepel M, and Sorger PK (2017a). Alternative drug sensitivity metrics improve preclinical cancer pharmacogenomics. Nat. Biotechnol 35, 500–502. [PubMed: 28591115]

Hafner M, Niepel M, Subramanian K, and Sorger PK (2017b). Designing Drug-Response Experiments and Quantifying their Results. Curr. Protoc. Chem. Biol 9.

Herrera-Abreu MT, Palafox M, Asghar U, Rivas MA, Cutts RJ, Garcia-Murillas I, Pearson A, Guzman M, Rodriguez O, Grueso J, et al. (2016). Early Adaptation and Acquired Resistance to CDK4/6 Inhibition in Estrogen Receptor–Positive Breast Cancer. Cancer Res 76, 2301–2313. [PubMed: 27020857]

Horn H, Schoof EM, Kim J, Robin X, Miller ML, Diella F, Palma A, Cesareni G, Jensen LJ, and Linding R (2014). KinomeXplorer: an integrated platform for kinome biology studies. Nat. Methods 11, 603–604. [PubMed: 24874572]

Hornbeck PV, Kornhauser JM, Tkachev S, Zhang B, Skrzypek E, Murray B, Latham V, and Sullivan M (2012). PhosphoSitePlus: A comprehensive resource for investigating the structure and function of experimentally determined post-translational modifications in man and mouse. Nucleic Acids Res 40.

Hortobagyi GN, Stemmer SM, Burris HA, Yap Y-S, Sonke GS, Paluch-Shimon S, Campone M, Blackwell KL, André F, Winer EP, et al. (2016). Ribociclib as First-Line Therapy for HR-Positive, Advanced Breast Cancer. N. Engl. J. Med 375, 1738–1748. [PubMed: 27717303]

Kettenbach AN, and Gerber SA (2011). Rapid and Reproducible Single-Stage Phosphopeptide Enrichment of Complex Peptide Mixtures: Application to General and Phosphotyrosine-Specific Phosphoproteomics Experiments. Anal. Chem 83, 7635–7644. [PubMed: 21899308]

Kim S, Tiedt R, Loo A, Horn T, Delach S, Kovats S, Haas K, Engstler BS, Cao A, Pinzon-Ortiz M, et al. (2018). The potent and selective cyclin-dependent kinases 4 and 6 inhibitor ribociclib (LEE011) is a versatile combination partner in preclinical cancer models. Oncotarget 9, 35226–35240. [PubMed: 30443290]

Kitada S, Zapata JM, Andreeff M, and Reed JC (2000). Protein kinase inhibitors flavopiridol and 7-hydroxy-staurosporine down-regulate antiapoptosis proteins in B-cell chronic lymphocytic leukemia. Blood 96, 393–397. [PubMed: 10887097]

Klaeger S, Heinzlmeir S, Wilhelm M, Polzer H, Vick B, Koenig P-A, Reinecke M, Ruprecht B, Petzoldt S, Meng C, et al. (2017). The target landscape of clinical kinase drugs. Science 358.

Knudsen ES, Hutcheson J, Vail P, Witkiewicz AK, Knudsen ES, Hutcheson J, Vail P, and Witkiewicz AK (2017). Biological specificity of CDK4/6 inhibitors: dose response relationship, in vivo signaling, and composite response signature. Oncotarget 8, 43678–43691. [PubMed: 28620137]

Kuleshov MV, Jones MR, Rouillard AD, Fernandez NF, Duan Q, Wang Z, Koplev S, Jenkins SL, Jagodnik KM, Lachmann A, et al. (2016). Enrichr: a comprehensive gene set enrichment analysis web server 2016 update. Nucleic Acids Res 44, W90–W97. [PubMed: 27141961]

Lamb J, Crawford ED, Peck D, Modell JW, Blat IC, Wrobel MJ, Lerner J, Brunet J-P, Subramanian A, Ross KN, et al. (2006). The Connectivity Map: using gene-expression signatures to connect small molecules, genes, and disease. Science 313, 1929–1935. [PubMed: 17008526]

Lim JSJ, Turner NC, and Yap TA (2016). CDK4/6 Inhibitors: Promising Opportunities beyond Breast Cancer. Cancer Discov 6, 697–699. [PubMed: 27371575]

Lin J-R, Izar B, Mei S, Wang S, Shah P, and Sorger P (2017). A simple open-source method for highly multiplexed imaging of single cells in tissues and tumours. BioRxiv.

Luen S, Virassamy B, Savas P, Salgado R, and Loi S (2016). The genomic landscape of breast cancer and its interaction with host immunity. Breast 29, 241–250. [PubMed: 27481651]

McAlister GC, Huttlin EL, Haas W, Ting L, Jedrychowski MP, Rogers JC, Kuhn K, Pike I, Grothe RA, Blethrow JD, et al. (2012). Increasing the multiplexing capacity of TMTs using reporter ion isotopologues with isobaric masses. Anal. Chem 84, 7469–7478. [PubMed: 22880955]

McAlister GC, Nusinow DP, Jedrychowski MP, Wühr M, Huttlin EL, Erickson BK, Rad R, Haas W, and Gygi SP (2014). MultiNotch MS3 enables accurate, sensitive, and multiplexed detection of differential expression across cancer cell line proteomes. Anal. Chem 86, 7150–7158. [PubMed: 24927332]

McCain J (2015). First-in-Class CDK4/6 Inhibitor Palbociclib Could Usher in a New Wave of Combination Therapies for HR+, HER2- Breast Cancer. P T Peer-Rev. J. Formul. Manag 40, 511–520.

McCarthy DJ, Chen Y, and Smyth GK (2012). Differential expression analysis of multifactor RNA-Seq experiments with respect to biological variation. Nucleic Acids Res 40, 4288–4297. [PubMed: 22287627]

Médard G, Pachl F, Ruprecht B, Klaeger S, Heinzlmeir S, Helm D, Qiao H, Ku X, Wilhelm M, Kuehne T, et al. (2015). Optimized Chemical Proteomics Assay for Kinase Inhibitor Profiling. J. Proteome Res 14, 1574–1586. [PubMed: 25660469]

Meloche S, and Pouysségur J (2007). The ERK1/2 mitogen-activated protein kinase pathway as a master regulator of the G1- to S-phase transition. Oncogene 26, 3227–3239. [PubMed: 17496918]

Nomanbhoy TK, Sharma G, Brown H, Wu J, Aban A, Vogeti S, Alemayehu S, Sykes M, Rosenblum JS, and Kozarich JW (2016). Chemoproteomic Evaluation of Target Engagement by the Cyclin-Dependent Kinase 4 and 6 Inhibitor Palbociclib Correlates with Cancer Cell Response. Biochemistry 55, 5434–5441. [PubMed: 27571378]

O'Brien N, Conklin D, Beckmann R, Luo T, Chau K, Thomas J, Mc Nulty A, Marchal C, Kalous O, von Euw E, et al. (2018). Preclinical Activity of Abemaciclib Alone or in Combination with Antimitotic and Targeted Therapies in Breast Cancer. Mol. Cancer Ther 17, 897 LP–907. [PubMed: 29483214]

O'Brien NA, Tomaso ED, Ayala R, Tong L, Issakhanian S, Linnartz R, Finn RS, Hirawat S, and Slamon DJ (2014). Abstract 4756: In vivo efficacy of combined targeting of CDK4/6, ER and PI3K signaling in ER+ breast cancer. Cancer Res 74, 4756–4756.

O'Leary B, Finn RS, and Turner NC (2016). Treating cancer with selective CDK4/6 inhibitors. Nat. Rev. Clin. Oncol 13, 417–430. [PubMed: 27030077]

Palechor-Ceron N, Suprynowicz FA, Upadhyay G, Dakic A, Minas T, Simic V, Johnson M, Albanese C, Schlegel R, and Liu X (2013). Radiation Induces Diffusible Feeder Cell Factor(s) That Cooperate with ROCK Inhibitor to Conditionally Reprogram and Immortalize Epithelial Cells. Am. J. Pathol 183, 1862–1870. [PubMed: 24096078]

Patnaik A, Rosen LS, Tolaney SM, Tolcher AW, Goldman JW, Gandhi L, Papadopoulos KP, Beeram M, Rasco DW, Hilton JF, et al. (2016a). Efficacy and Safety of Abemaciclib, an Inhibitor of CDK4 and CDK6, for Patients with Breast Cancer, Non–Small Cell Lung Cancer, and Other Solid Tumors. Cancer Discov 6.

Patnaik A, Rosen Lee.S., Tolaney Sara.M., Tolcher Anthony.W., and Goldman Jonathan.W. (2016b). Single-Agent Abemaciclib Active in Breast Cancer. Cancer Discov 6, 809–810.

Paulo JA, McAllister FE, Everley RA, Beausoleil SA, Banks AS, and Gygi SP (2015). Effects of MEK inhibitors GSK1120212 and PD0325901 in vivo using 10-plex quantitative proteomics and phosphoproteomics. Proteomics 15, 462–473. [PubMed: 25195567]

Peplow M (2017). Astex shapes CDK4/6 inhibitor for approval. Nat. Biotechnol 35, 395–396. [PubMed: 28486460]

Rappsilber J, Mann M, and Ishihama Y (2007). Protocol for micro-purification, enrichment, pre-fractionation and storage of peptides for proteomics using StageTips. Nat. Protoc 2, 1896–1906. [PubMed: 17703201]

Raub TJ, Wishart GN, Kulanthaivel P, Staton BA, Ajamie RT, Sawada GA, Gelbert LM, Shannon HE, Sanchez-Martinez C, and De Dios A (2015). Brain Exposure of Two Selective Dual CDK4 and CDK6 Inhibitors and the Antitumor Activity of CDK4 and CDK6 Inhibition in Combination with Temozolomide in an Intracranial Glioblastoma Xenograft. Drug Metab. Dispos 43, 1360 LP–1371. [PubMed: 26149830]

Reid Y, Storts D, Riss T, and Minor L (2004). Authentication of Human Cell Lines by STR DNA Profiling Analysis.

Riley NM, and Coon JJ (2016). Phosphoproteomics in the Age of Rapid and Deep Proteome Profiling. Anal. Chem 88, 74–94. [PubMed: 26539879]

Robinson MD, McCarthy DJ, and Smyth GK (2010). edgeR: a Bioconductor package for differential expression analysis of digital gene expression data. Bioinformatics 26, 139–140. [PubMed: 19910308]

Schwanhäusser B, Busse D, Li N, Dittmar G, Schuchhardt J, Wolf J, Chen W, and Selbach M (2011). Global quantification of mammalian gene expression control. Nature 473, 337. [PubMed: 21593866]

Sherr CJ, Beach D, and Shapiro GI (2016). Targeting CDK4 and CDK6: From Discovery to Therapy. Cancer Discov 6, 353–367. [PubMed: 26658964]

Sledge GW, Toi M, Neven P, Sohn J, Inoue K, Pivot X, Burdaeva O, Okera M, Masuda N, Kaufman PA, et al. (2017). MONARCH 2: Abemaciclib in Combination With Fulvestrant in Women With HR+/HER2- Advanced Breast Cancer Who Had Progressed While Receiving Endocrine Therapy. J. Clin. Oncol. Off. J. Am. Soc. Clin. Oncol. JCO2017737585.

Soumillon M, Cacchiarelli D, Semrau S, van Oudenaarden A, and Mikkelsen TS (2014). Characterization of directed differentiation by high-throughput single-cell RNA-Seq. BioRxiv.

Srivastava A, Sarkar H, Gupta N, and Patro R (2016). RapMap: a rapid, sensitive and accurate tool for mapping RNA-seq reads to transcriptomes. Bioinforma. Oxf. Engl 32, i192–i200.

Subramanian A, Tamayo P, Mootha VK, Mukherjee S, Ebert BL, Gillette MA, Paulovich A, Pomeroy SL, Golub TR, Lander ES, et al. (2005). Gene set enrichment analysis: A knowledge-based approach for interpreting genome-wide expression profiles. Proc. Natl. Acad. Sci 102, 15545–15550. [PubMed: 16199517]

Sumi NJ, Kuenzi BM, Knezevic CE, Remsing Rix LL, and Rix U (2015). Chemoproteomics Reveals Novel Protein and Lipid Kinase Targets of Clinical CDK4/6 Inhibitors in Lung Cancer. ACS Chem. Biol 10, 2680–2686. [PubMed: 26390342]

Svensson V, Natarajan KN, Ly L-H, Miragaia RJ, Labalette C, Macaulay IC, Cvejic A, and Teichmann SA (2017). Power analysis of single-cell RNA-sequencing experiments. Nat. Methods 14, 381. [PubMed: 28263961]

Ting L, Rad R, Gygi SP, and Haas W (2011). MS3 eliminates ratio distortion in isobaric multiplexed quantitative proteomics. Nat. Methods 8, 937–940. [PubMed: 21963607]

Toogood PL, Harvey PJ, Repine JT, Sheehan DJ, VanderWel SN, Zhou H, Keller PR, McNamara DJ, Sherry D, Zhu T, et al. (2005). Discovery of a potent and selective inhibitor of cyclin-dependent kinase 4/6. J. Med. Chem 48, 2388–2406. [PubMed: 15801831]

Torres-guzmán R, Calsina B, Hermoso A, Baquero C, Amat J, Mcnulty AM, Gong X, and Boehnke K (2017). Preclinical characterization of abemaciclib in hormone receptor positive breast cancer.

Turner NC, Liu Y, Zhu Z, Loi S, Colleoni M, Loibl S, DeMichele A, Harbeck N, André F, Bayar MA, et al. (2019). Cyclin E1 Expression and Palbociclib Efficacy in Previously Treated Hormone Receptor-Positive Metastatic Breast Cancer. J. Clin. Oncol. Off. J. Am. Soc. Clin. Oncol. JCO1800925.

Wittmann S, Bali P, Donapaty S, Nimmanapalli R, Guo F, Yamaguchi H, Huang M, Jove R, Wang HG, and Bhalla K (2003). Flavopiridol down-regulates antiapoptotic proteins and sensitizes human breast cancer cells to epothilone B-induced apoptosis. Cancer Res 63, 93–99. [PubMed: 12517783]

Yang C, Li Z, Bhatt T, Dickler M, Giri D, Scaltriti M, Baselga J, Rosen N, and Chandarlapaty S (2017). Acquired CDK6 amplification promotes breast cancer resistance to CDK4/6 inhibitors and loss of ER signaling and dependence. Oncogene 36, 2255–2264. [PubMed: 27748766]

SIGNIFICANCE

The integration of multiple cell-based and *in vitro* kinome profiling methods has enabled systematic comparison of the target spectra of three recently approved CDK4/6 inhibitors – palbociclib, ribociclib, and abemaciclib – regarded as breakthroughs in the treatment of HR+ breast cancer. We find that abemaciclib has a substantially wider range of inhibitory activities than other CDK4/6 inhibitors, providing a rationale for treating patients with abemaciclib following disease progression on palbociclib or ribociclib. Breast cancer cells that are resistant to palbociclib and ribociclib, including cells derived from a patient whose cancer progressed on ribociclib plus letrozole, remain sensitive to abemaciclib at concentrations of 0.3 μM and above, overlapping human C_{max} concentrations. We have identified one patient who has benefitted directly from treatment with single agent abemaciclib after first responding and then becoming resistant to palbociclib plus fulvestrant, and our data suggest that other patients may also benefit from such a change in therapy. The possibilities for use of abemaciclib in tumors that are pRb-deficient remain less certain, since drug activity is observed only at micromolar concentrations in pRb-deficient cell lines. A final possibility suggested by this work is that it might be advantageous to combine CDK4/6 inhibitors with drugs that inhibit secondary targets of abemaciclib such as CDK2 (a strategy Pfizer is pursuing in a single molecule, US patent 20180044344A1). Our work shows that polypharmacology can be exploited in a molecule such as abemaciclib to achieve more durable responses than with "pure" CDK4/6 inhibitors such as ribociclib. More generally, our findings demonstrate the value of systematic comparative target profiling of approved and late stage human therapeutics developed against the same target(s) but having different chemical structures.
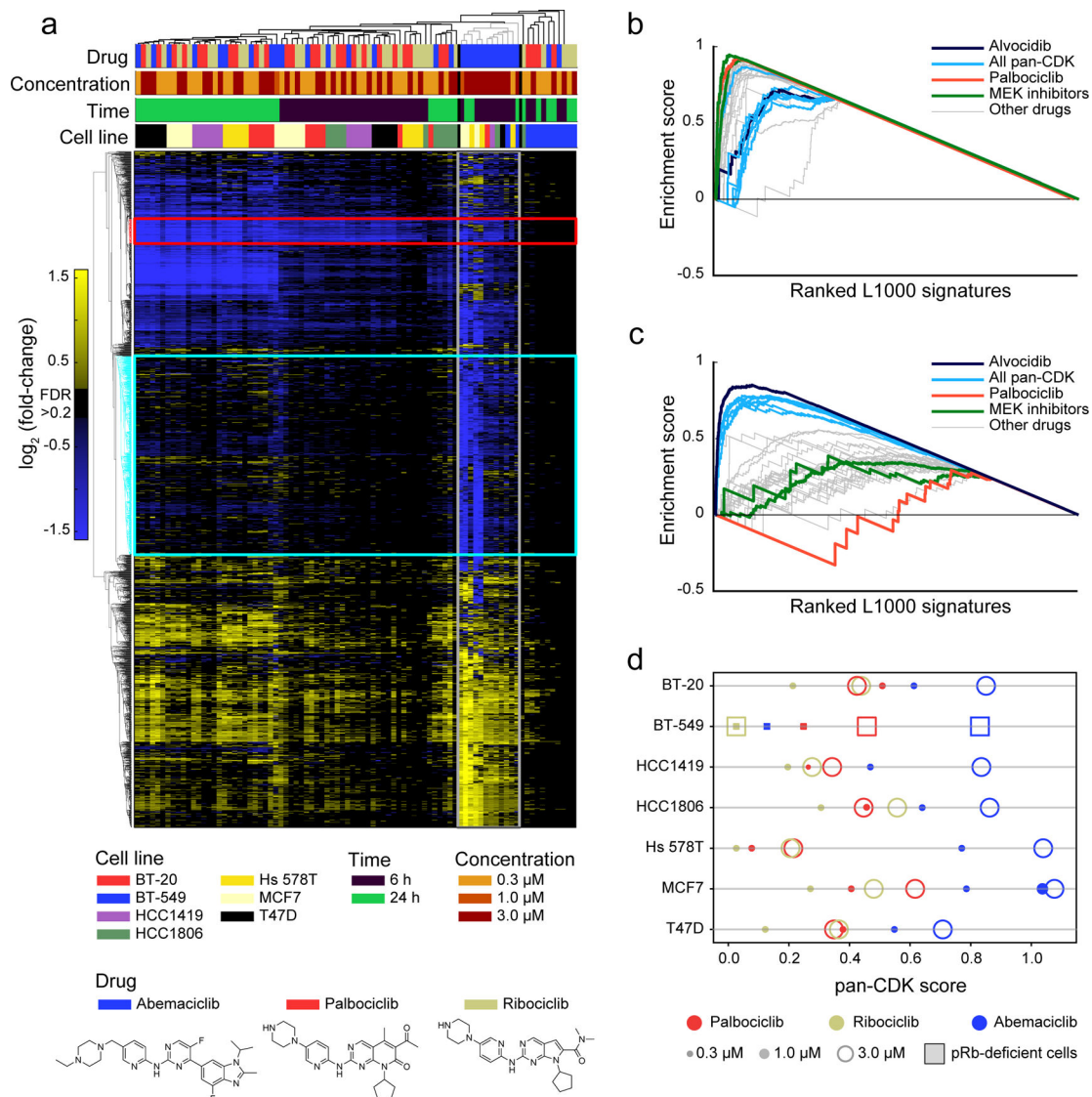
Figure 1: Transcriptional responses of breast cancer cell lines to CDK4/6 inhibitors.
(a) Clustering of transcriptional responses for seven breast cancer cell lines treated for 6 or 24 hours with ribociclib, palbociclib, or abemaciclib at 0.3, 1, or 3 μM. Only genes for which statistically significant (FDR < 0.2) changes were observed in at least 3 conditions are shown. Down-regulated genes comprising signature 1 and 2 are outlined in red and cyan, respectively, and the gray box denotes the cluster containing expression profiles with the highest signature 2 scores. **(b-c)** Enrichment scores for signature 1 (b) and 2 (c) based on L1000 signatures identified by Enrichr (see STAR Methods). **(d)** Score of the pan-CDK transcriptional signature per cell line following six hours of exposure to drug based on RNA-seq data from panel (a).
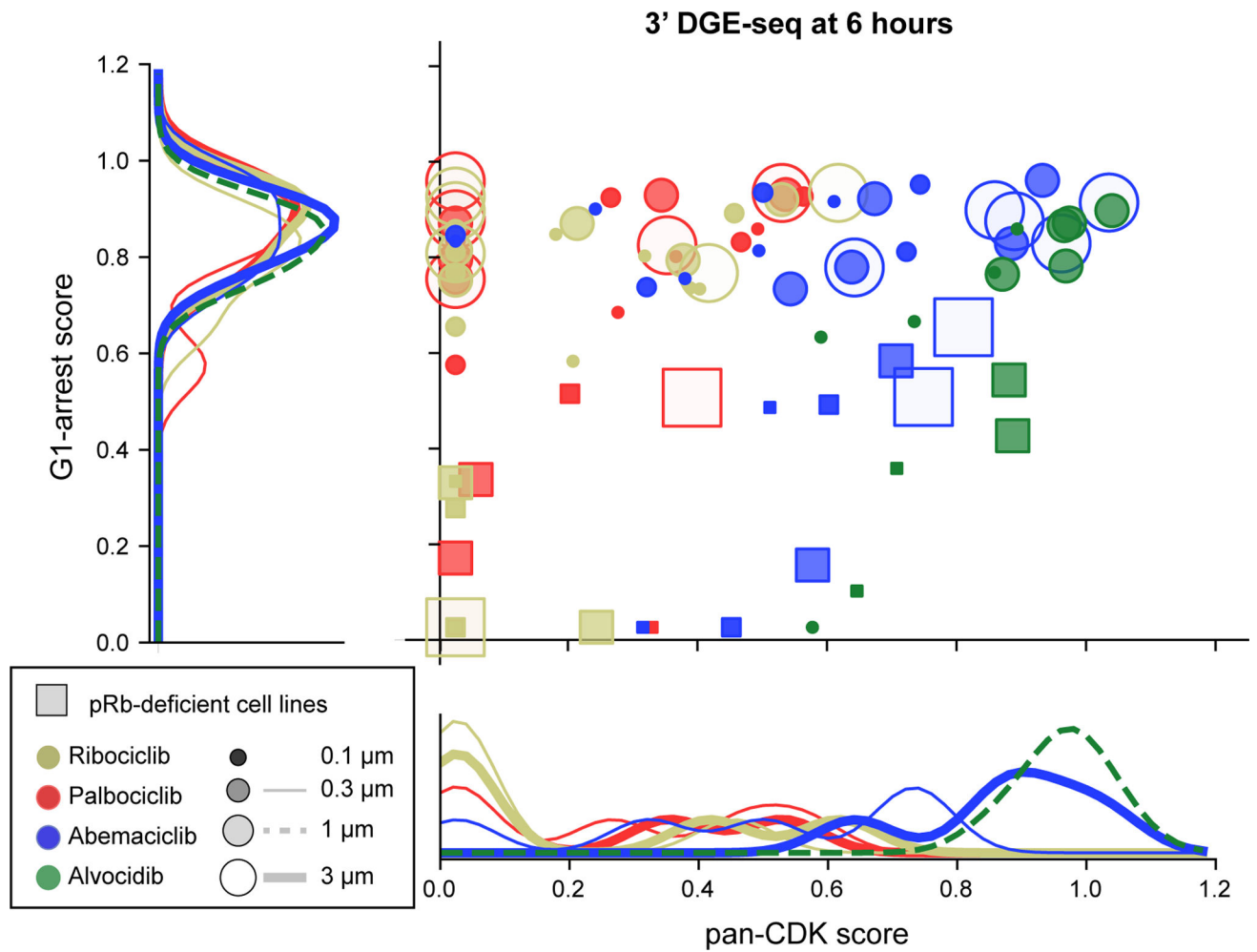
Figure 2: G1-arrest and pan-CDK scores induced by CDK4/6 inhibitors.
Score of the G1-arrest signature relative to the pan-CDK signature for seven cell lines treated with palbociclib, ribociclib, abemaciclib, or alvociclib at 0.1, 0.3, 1, or 3 μM; squares denote pRb-deficient lines. Distributions of scores for pRb-competent lines are shown at the margins for each signature.
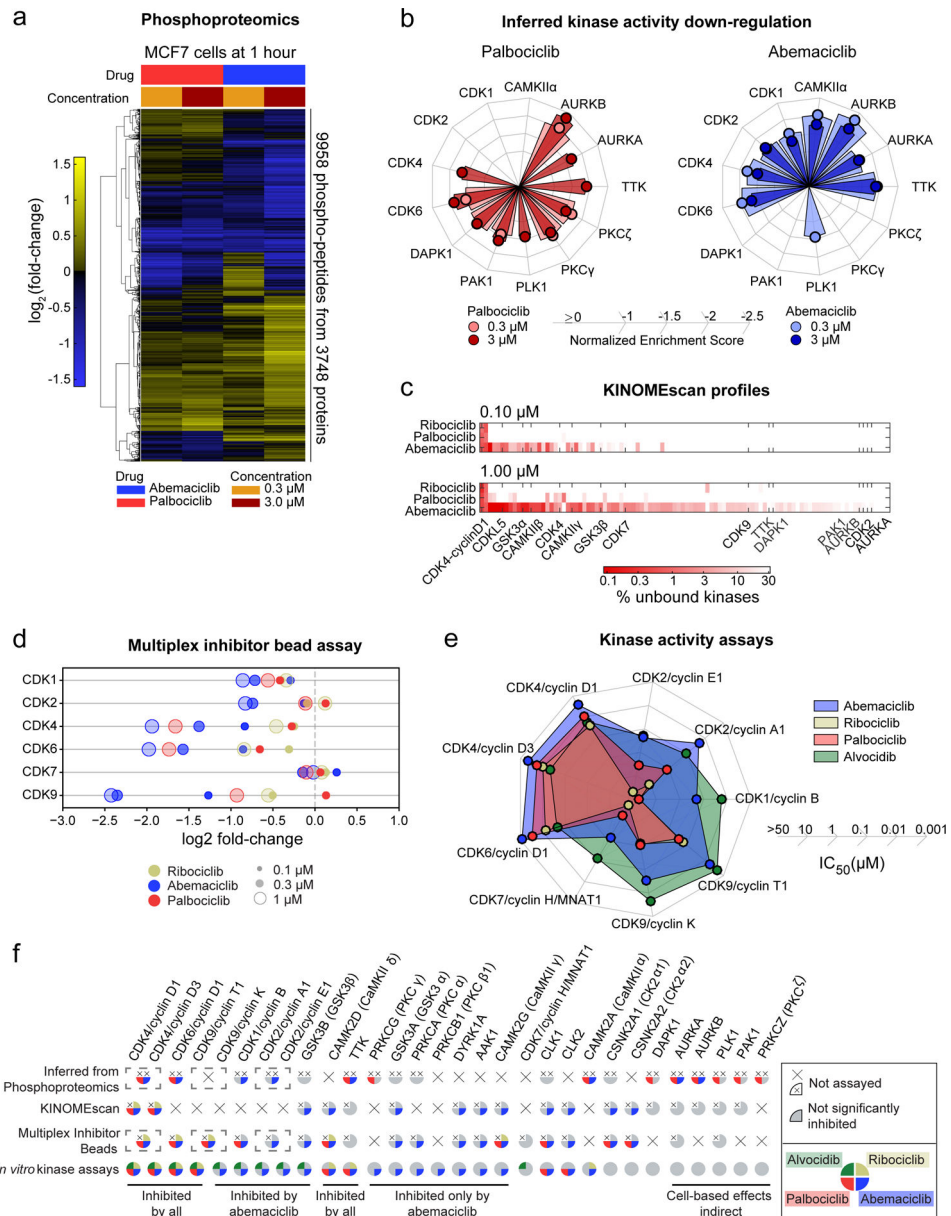
Figure 3: Inhibition of CDK/cyclin activity by CDK4/6 inhibitors.
(a) Clustering of changes in phosphopeptide levels for MCF7 cells treated for 1 hour with either abemaciclib or palbociclib at 0.3 or 3 μM. **(b)** Normalized enrichment scores for kinases based on the phosphoproteomic data in panel (a). Only kinases inferred as significantly down-regulated (FDR < 0.2) in at least two conditions are shown. **(c)** Fraction of unbound kinases at 0.1 and 1 μM of each CDK4/6 inhibitor as measured by the KINOMEscan assay for the top 100 bound kinases plus kinases inferred in (b) (see Figure S2). CAMKIIα, CDK6, PKCγ, and PKCζ were not present in the panel. **(d)** Degree of inhibition (log$_2$ fold change) of each CDK as detected by MIB/MS after treating a mixed cell lysate with a CDK4/6 inhibitor at the doses indicated. **(e)** IC_{50} values for CDK/cyclin complexes for CDK4/6 inhibitors and alvocidib as measured using purified kinases *in vitro*

(see Figure S3). **(f)** Summary of kinases that were assayed by phosphoproteomics, KINOMEscan, MIB/MS, and SelectScreen. Each slice of the pie represents inhibition by abemaciclib, ribociclib, palbociclib, or alvocidib. For each assay, slices are colored only if the corresponding drug substantially inhibited the kinases (defined as FDR < 0.2 for phosphoproteomic inference, 90% inhibition at 1 μM drug by KINOMEscan, $\log_2$ fold-change < −0.45 for MIB/MS, or IC_{50} < 0.5 μM by in vitro kinase assays). An 'x' inside a slice denotes that that drug was not profiled in that assay. A large 'X' in place of a pie indicates that that kinase was not profiled in that assay. Bound complexes such as CDK4/ cyclin D1 or CDK4/cyclin D3 cannot be disambiguated in kinase inference and MIB/MS assays and are therefore depicted as a single entity within a box.
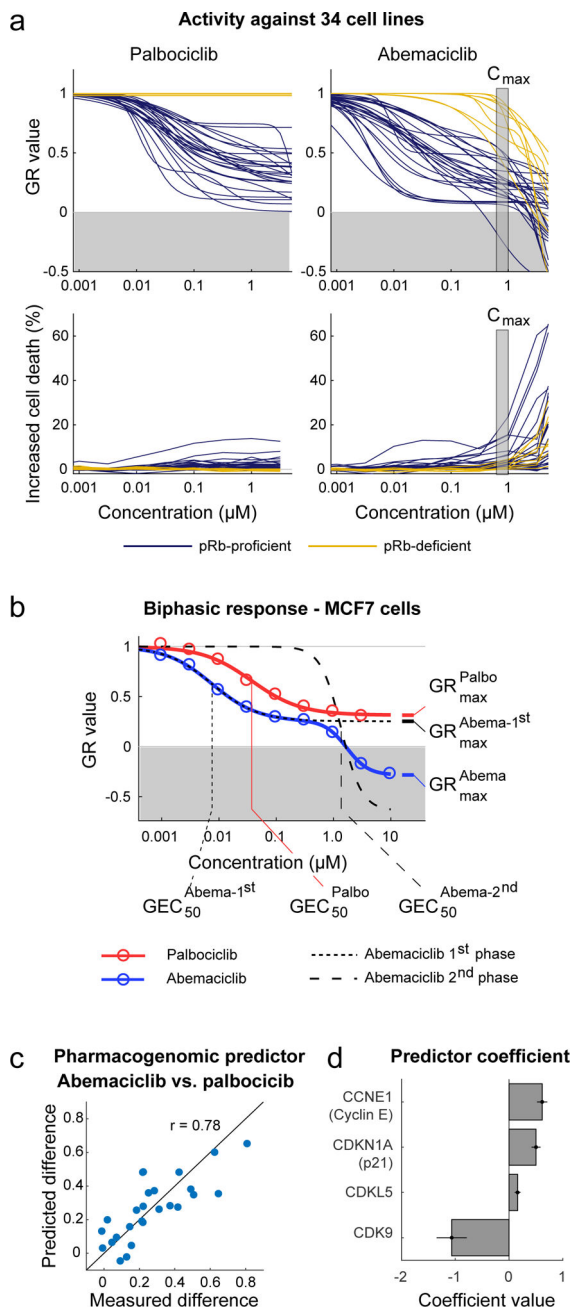
Figure 4: Comparison of the phenotypic response of breast cancer cell lines to CDK4/6 inhibitors.

(a) GR curves for cell growth (top) and increase of dead cells relative to a vehicle-only control (bottom) for 26 pRb-proficient breast cancer cell lines (blue) and 8 pRb-deficient cell lines (yellow) treated with palbociclib (left) or abemaciclib (right) for 72 hours. The vertical box illustrates the maximum serum concentration for abemaciclib (C_{max}). **(b)** Dose-response curve for palbociclib (red) and abemaciclib (blue) in MCF7 cells. Dotted lines depict two fitted sigmoidal curves whose product optimally recapitulates the blue curve with extracted values for GEC_{50} (50%-maximal effective concentration) shown below and for GR_{max} (maximal efficacy) shown to the right (See Figure S4). **(c-d)** Performance of a

pharmacogenomic predictor of palbociclib vs. abemaciclib drug response constructed from data on mRNA levels for 30 cell cycle regulators; (c) shows the observed versus predicted (leave-one-out cross validation) difference in GR value at 3 μM between palbociclib and abemaciclib based on a linear model containing the expression of four genes, whose coefficients are shown in (d); error bars represent the standard error of the model.
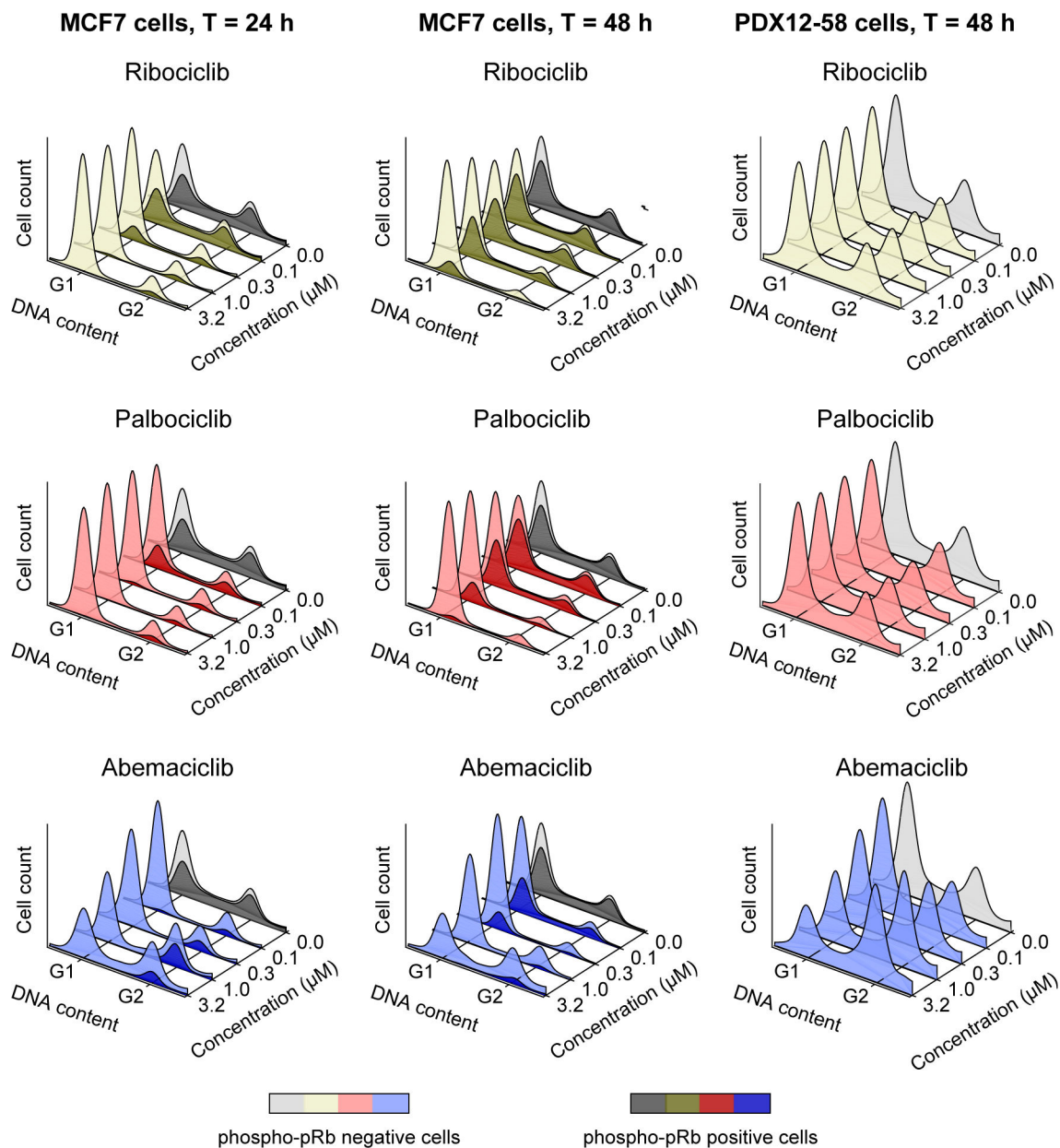
Figure 5: Comparison of the effects of ribociclib, palbociclib, and abemaciclib on the cell cycle.
Distribution of DNA content in MCF7 cells exposed to one of three CDK4/6 inhibitors over a range of concentrations for 24 (left) or 48 (middle) hours, and in PDX-1258 cells, which are pRb-deficient, exposed to the same conditions for 48 hours (right). In each curve the phospho-pRb positive cell population is depicted in a darker shade. One representative replicate out of three is shown.
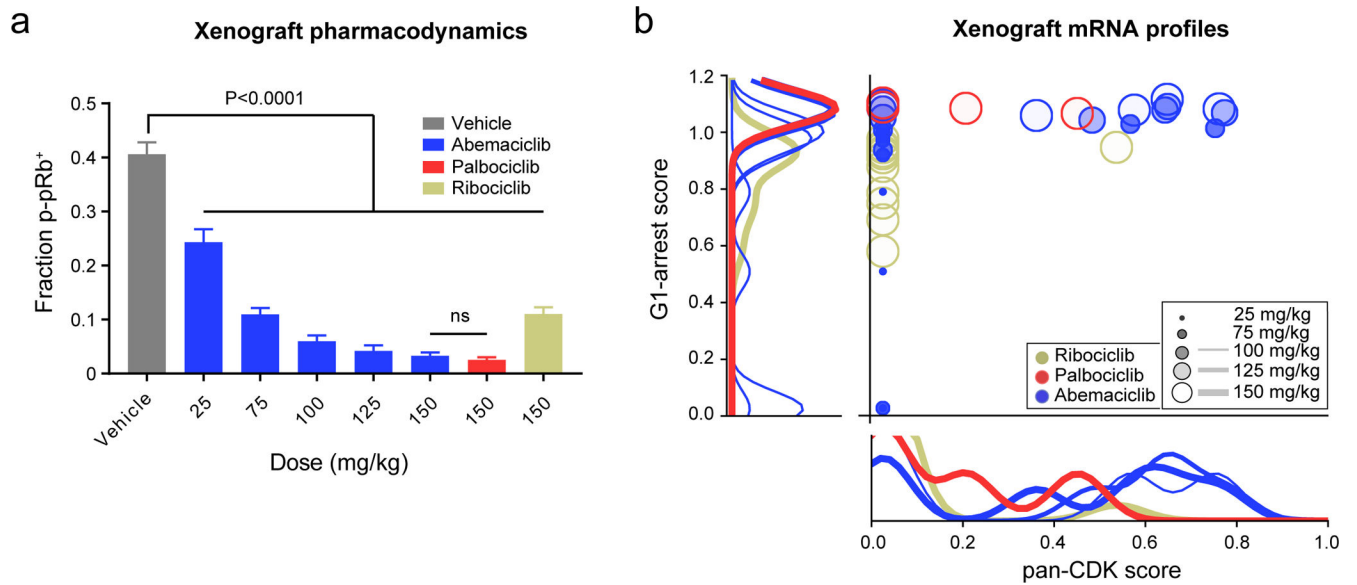
Figure 6: Transcriptional response of MCF-7 xenografted cells to CDK4/6 inhibitors
(a) Fraction of phospho-pRb positive tumor cells in MCF-7 xenografts after four days of CDK4/6 inhibitor treatment. **(b)** Score of the pan-CDK transcriptional signature as compared to the G1-arrest signature across MCF-7 tumors following four days of exposure to drug; same analysis as in Figure 2.
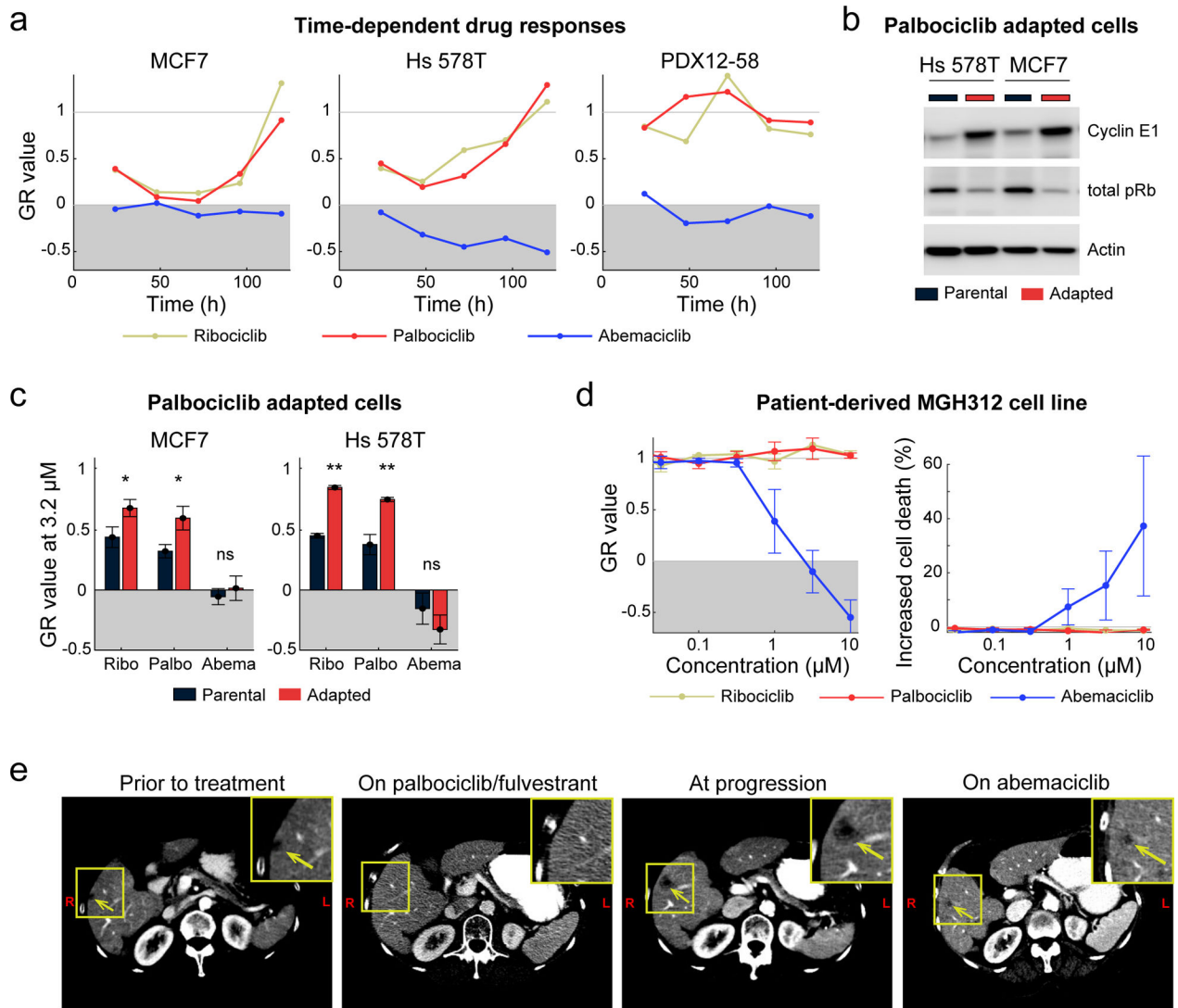
Figure 7: Acute and adaptive responses of breast cancer cell lines and tumors to CDK4/6 inhibitors.

(a) Time-dependent GR values for MCF7, Hs 578T, and PDX12–58 cells treated with 3.16 μM ribociclib, palbociclib, or abemaciclib for up to five days. One representative replicate out of four is shown. **(b)** Western Blots of cyclin E and total pRb levels in Hs 578T and MCF7 parental cells and in cells adapted to grow in 1 μM palbociclib. **(c)** GR values for Hs 578T and MCF7 parental cells and cells adapted to grow in 1 μM palbociclib following exposure to 3.16 μM ribociclib, palbociclib, or abemaciclib for 72 h (see Figure S7); * denotes $P < 0.05$ and ** $P < 0.01$ as measured using a t-test with six replicates in each group. Error bars denote SEM of six replicates. **(d)** GR values (left) and increase in dead cells relative to a vehicle-only control (right) for the patient-derived line MGH312 in response to 96-hour exposure to ribociclib, palbociclib, or abemaciclib. Error bars show the SEM of three replicates. **(e)** CT scan of patient with metastatic HR+/HER2- breast cancer showing a liver lesion prior to palbociclib/fulvestrant treatment (1st panel); upon complete radiographic regression of the lesion following 7 months of palbociclib/fulvestrant treatment

(2nd panel); reappearance of the lesion after 20 months on palbociclib/fulvestrant (3rd panel); and regression of the lesion 3 months after a switch to treatment with abemaciclib (last panel).

KEY RESOURCES TABLE

REAGENT or RESOURCE	SOURCE	IDENTIFIER
Antibodies		
Phospho-pRb (Ser807/811) (clone D20B12) Alexa 555	Cell Signaling Technologies	Cat # 8957; RRID AB_2728827
pRb (clone 4H1)	Cell Signaling Technologies	Cat # 9309; RRID AB_823629
Cyclin E1 (clone HE12)	Cell Signaling Technologies	Cat # 4129; RRID AB_2071200
β-Actin (clone 8H10D10)	Cell Signaling Technologies	Cat # 3700; RRID AB_10985704
Anti-mouse IgG, HRP-linked	Cell Signaling Technologies	Cat # 7076; RRID AB_330924
Vimentin (clone D21H3) Alexa 555	Cell Signaling Technologies	Cat # 9855; RRID AB_10859896
E-cadherin (clone 24E10) Alexa 488	Cell Signaling Technologies	Cat # 3199; RRID AB_823441
Chemicals, Peptides, and Recombinant Proteins		
Palbociclib	MedChem Express	Cat # HY-50767, batch # 16349
Abemaciclib	MedChem Express	Cat # HY-16297, batch # 08492
Ribociclib	MedChem Express	Cat # HY-15777, batch # 11003
Alvocidib	Haoyuan chemexpress	Cat # HY-10005, batch # HY-009_TM-20090429
Fetal bovine serum	Life Technologies	26140–079
Horse Serum	Life Technologies	16050–122
Penicillin/Streptomycin	Corning	30–002-Cl
Epidermal growth factor	PeproTech	AF-100–15
Insulin	Sigma Aldrich	I1882
Hydrocortisone	Sigma Aldrich	H0888
Cholera toxin	Sigma Aldrich	C8052
Y-27632	Enzo Life Sciences	ALX-270–333-M025
Critical Commercial Assays		
KINOMEscan	DiscoverX	SCANmax
SelectScreen Z' lyte	Life Technologies	Z'Lyte
SelectScreen Lantha	Life Technologies	Lantha
SelectScreen Adapta	Life Technologies	Adapta
TruSeq kit	Illumina	Cat # 20019792
Deposited Data		
mRNAseq on cell lines	This paper	GEO GSE99116
Phosphoproteomics	This paper	Synapse syn18488089
Dose response	This paper	LINCS DB 20343, 20344
3' DGEseq on cell lines	This paper	GEO GSE125215
mRNAseq on xenografts	This paper	GEO GSE124854
Experimental Models: Cell Lines		
BT20	ATCC	HTB-19; RRID CVCL_0178
BT549	ATCC	HTB-122; RRID CVCL_1092
CAL120	DSMZ	ACC 459; RRID CVCL_1104

REAGENT or RESOURCE	SOURCE	IDENTIFIER
CAL51	DSMZ	ACC 302; RRID CVCL_1110
CAL851	DSMZ	ACC 440; RRID CVCL_1114
CAMA1	ATCC	HTB-21; RRID CVCL_1115
HCC1143	ATCC	CRL-2321; RRID CVCL_1245
HCC1395	ATCC	CRL-2324; RRID CVCL_1249
HCC1419	ATCC	CRL-2326; RRID CVCL_1251
HCC1428	ATCC	CRL-2327; RRID CVCL_1252
HCC1500	ATCC	CRL-2329; RRID CVCL_1254
HCC1806	ATCC	CRL-2335; RRID CVCL_1258
HCC1937	ATCC	CRL-2336; RRID CVCL_0290
HCC1954	ATCC	CRL-2338; RRID CVCL_1259
HCC38	ATCC	CRL-2314; RRID CVCL_1267
HCC70	ATCC	CRL-2315; RRID CVCL_1270
HME1	ATCC	CRL-4010; RRID CVCL_3383
HS578T	ATCC	HTB-126; RRID CVCL_0332
MCF10A	ATCC	CRL-10317; RRID CVCL_0598
MCF7	ATCC	HTB-22; RRID CVCL_0031
MDAMB157	ATCC	HTB-24; RRID CVCL_0618
MDAMB231	ATCC	HTB-26; RRID CVCL_0062
MDAMB361	ATCC	HTB-27; RRID CVCL_0620
MDAMB436	ATCC	HTB-130; RRID CVCL_0623
MDAMB453	ATCC	HTB-131; RRID CVCL_0418
MDAMB468	ATCC	HTB-132; RRID CVCL_0419
MGH312	MGH (Crystal *et al.*, 2014)	N/A
PDX1258	Brugge lab	N/A
PDX1328	Sorger lab	N/A
PDXHCI002	Brugge lab	N/A
SKBR3	ATCC	HTB-30; RRID CVCL_0033
SUM1315	University of Michigan	SUM-1315MO2; RRID CVCL_5589
SUM149	Asterand	SUM-149PT; RRID CVCL_3422
SUM159	Asterand	SUM-159PT; RRID CVCL_5423
T47D	ATCC	HTB-133; RRID CVCL_0553
Software and Algorithms		
MATLAB (R2016b)	MathWorks	https://www.mathworks.com/products/matlab.html
Columbus (v2.7.0)	Perkin Elmer, Waltham, MA	http://www.perkinelmer.com/product/image-data-storage-and-analysis-system-columbus
bcbio-Nextgen toolkit (v1.0.3a)		https://github.com/chapmanb/bcbio-nextgen
edgeR v3.18.1 (R v3.2.1)	(Robinson, McCarthy and Smyth, 2010; McCarthy, Chen and Smyth, 2012)	https://bioconductor.org/packages/release/bioc/html/edgeR.html

REAGENT or RESOURCE	SOURCE	IDENTIFIER
Sequest (v28)	(Eng, McCormack and Yates, 1994)	http://fields.scripps.edu/yates/wp/
Kinase activity inference		https://github.com/datarail/msda